Mock-Walker Simulations: Mean Climates, Responses to Warming and Transition to Double-Cell Circulations

Nicholas Lutsko[1] and Timothy Wallace Cronin[2]

[1]Scripps Institution of Oceanography.
[2]MIT

February 9, 2023

Abstract

Improving understanding of the two-way interactions between clouds and large-scale atmospheric circulations requires modeling set-ups that can resolve cloud-scale processes, while also including representations of the circulations themselves. In this study, we investigate the potential for mock-Walker simulations to help untangle these interactions by assessing their ability to reproduce the observed climate over the equatorial Pacific. Mock-Walker simulations with realistic zonal sea-surface temperature (SST) gradients show qualitative similarities with reanalysis and satellite data, though notable differences include (1) the presence of double-celled overturning circulations, (2) extreme upper tropospheric dryness over the cold pools, and (3) substantially weaker longwave cloud radiative effects. The double-cell circulations are part of a transition from single to double cells as mean SST is increased, with the transition occurring near present day temperatures. The circulation changes dominate the response of mock-Walker simulations to warming, though their effects are smaller for relatively weak zonal SST gradients. Mock-Walker simulations also exhibit a wide range of climate sensitivities, due to cloud feedbacks that are strongly negative for larger SST gradients and strongly positive for weaker SST gradients. Finally, we show that radiative-subsidence balance can be used to explain the development of the double cells, but are unable to further explain the dynamics of the transition given the complex vertical profiles of stability and atmospheric radiative cooling in these simulations. Since Earth's present-day climate is close to our simulated transition to a double-celled circulation, these dynamics merit further investigation.

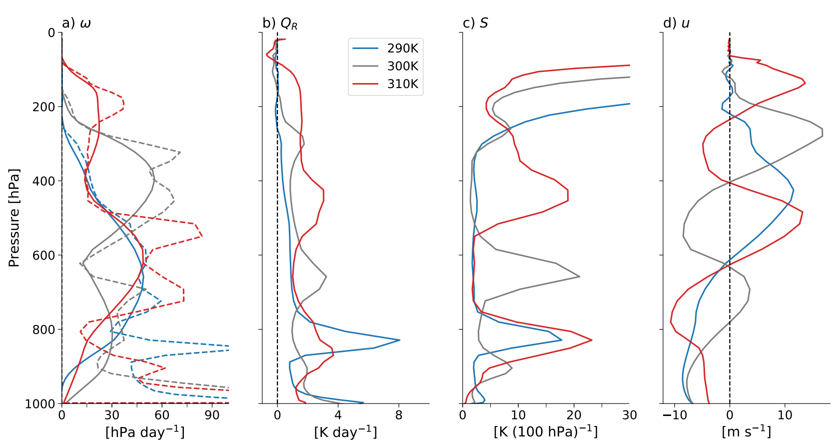

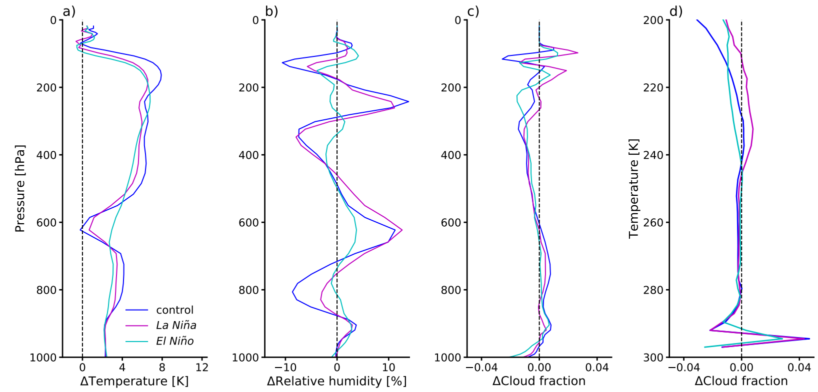
a)
b)
c)
d)
Pressure [hPa]
Temperature [K]
control
La Niña
El Niño
ΔTemperature [K]
ΔRelative humidity [%]
ΔCloud fraction
ΔCloud fraction

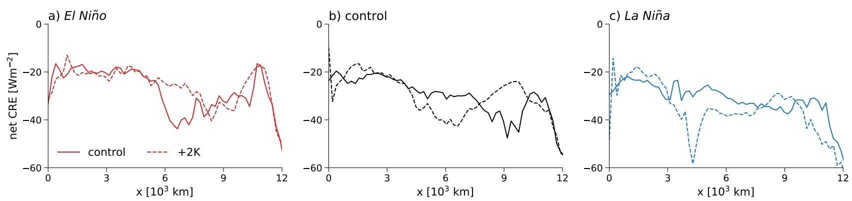
a) El Niño
b) control
c) La Niña
net CRE [Wm^{-2}]
control
+2K
x [10^3 km]
x [10^3 km]
x [10^3 km]

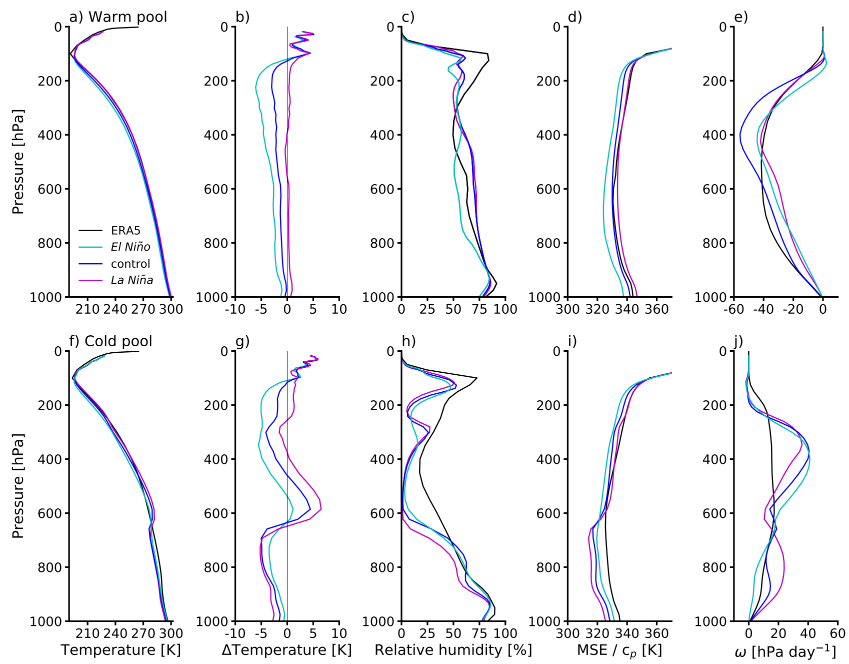
a) Warm pool
b)
c)
d)
e)
f) Cold pool
g)
h)
i)
j)
Pressure [hPa]
Pressure [hPa]
ERA5
El Niño
control
La Niña
Temperature [K]
ΔTemperature [K]
Relative humidity [%]
MSE / c$_p$ [K]
ω [hPa day^{-1}]

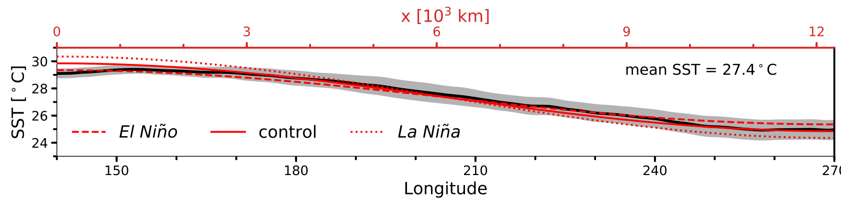
x [10^3 km]
SST [°C]
mean SST = 27.4 °C
El Niño
control
La Niña
Longitude

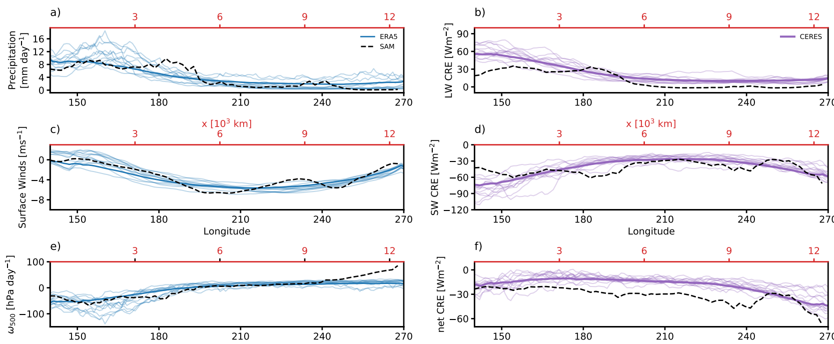
a)
b)
c)
d)
e)
f)
Precipitation [mm day^{-1}]
ERA5
SAM
LW CRE [Wm^{-2}]
CERES
Surface Winds [ms^{-1}]
x [10^3 km]
SW CRE [Wm^{-2}]
Longitude
ω_{500} [hPa day^{-1}]
net CRE [Wm^{-2}]

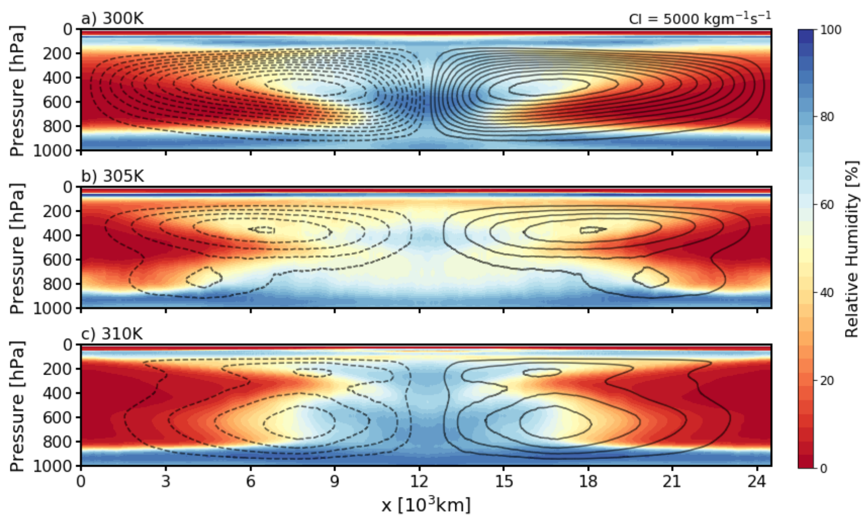
a) 300K
CI = 5000 kgm^{-1}s^{-1}
b) 305K
c) 310K
Pressure [hPa]
Relative Humidity [%]
x [10^3km]

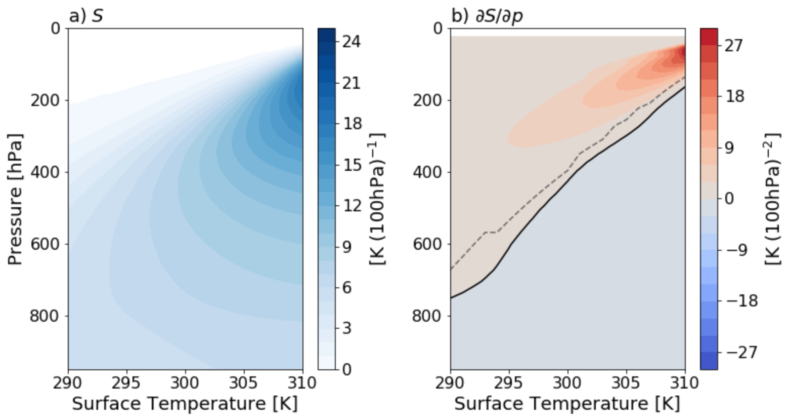
a) S
Pressure [hPa]
0
200
400
600
800
290
295
300
305
310
Surface Temperature [K]
24
21
18
15
12
9
6
3
0
[K (100hPa)$^{-1}$]
b) $\partial S/\partial p$
0
200
400
600
800
290
295
300
305
310
Surface Temperature [K]
27
18
9
0
−9
−18
−27
[K (100hPa)$^{-2}$]

Mock-Walker Simulations: Mean Climates, Responses to Warming and Transition to Double-Cell Circulations

Nicholas J. Lutsko[1], Timothy W. Cronin[2]

[1]Scripps Institution of Oceanography, University of California at San Diego, La Jolla, California

[2]Department of Earth, Atmospheric, and Planetary Sciences, Massachusetts Institute of Technology, Cambridge, Massachusetts

Key Points:

- Mock-Walker simulations compare favorably with the observed climate over the tropical Pacific, with some limitations
- The circulation transitions from a single-cell to a double-cell as the mean SST is increased
- Smaller zonal SST gradients produce more positive cloud feedbacks.

Corresponding author: Nicholas Lutsko, `nlutsko@ucsd.edu`

Abstract

Improving understanding of the two-way interactions between clouds and large-scale atmospheric circulations requires modeling set-ups that can resolve cloud-scale processes, while also including representations of the circulations themselves. In this study, we investigate the potential for mock-Walker simulations to help untangle these interactions by assessing their ability to reproduce the observed climate over the equatorial Pacific. Mock-Walker simulations with realistic zonal sea-surface temperature (SST) gradients show qualitative similarities with reanalysis and satellite data, though notable differences include (1) the presence of double-celled overturning circulations, (2) extreme upper tropospheric dryness over the cold pools, and (3) substantially weaker longwave cloud radiative effects. The double-cell circulations are part of a transition from single to double cells as mean SST is increased, with the transition occurring near present day temperatures. The circulation changes dominate the response of mock-Walker simulations to warming, though their effects are smaller for relatively weak zonal SST gradients. Mock-Walker simulations also exhibit a wide range of climate sensitivities, due to cloud feedbacks that are strongly negative for larger SST gradients and strongly positive for weaker SST gradients. Finally, we show that radiative-subsidence balance can be used to explain the development of the double cells, but are unable to further explain the dynamics of the transition given the complex vertical profiles of stability and atmospheric radiative cooling in these simulations. Since Earth's present-day climate is close to our simulated transition to a double-celled circulation, these dynamics merit further investigation.

Plain language summary

Untangling the coupled interactions between clouds and large-scale atmospheric flows is one of the "Grand Challenges" of climate science. Large-scale flows are the main control on the spatial distribution of cloud-types in the tropics, but clouds in turn play a key role in setting the strengths and spatial structures of these flows. Here, we investigate "mock-Walker" simulations as a potential idealized modeling set-up for investigating the two-way interactions between clouds and tropical circulations. Mock-Walker simulations include the zonal sea-surface temperature (SST) gradient needed to generate realistic tropical circulations, while using grid resolutions sufficient to partially resolve clouds. We compare these simulations with observations of the atmosphere above the tropical Pacific, finding that they qualitatively reproduce many aspects of the tropical climate, though with some notable differences. We also investigate the model's responses to varying SST gradients and to mean SST warming. In both cases, the responses are strongly influenced by circulation changes, which affect cloud distributions. Finally, we find that an El Niño like set-up has a high climate sensitivity, while a La Niña like set-up has a low climate sensitivity.

1 Introduction

How clouds change in a warmer world remains the largest uncertainty in projecting future climate change under a given emission scenario [e.g., *Soden and Held*, 2006; *Forster et al.*, 2013; *Vial et al.*, 2013; *Schneider et al.*, 2017; *Sherwood et al.*, 2020]. The reason for this is that cloud processes occur on scales that are too small for global climate models to resolve, so they must be represented by parameterizations, which suffer from both parametric and structural uncertainties as to whether they accurately represent the physics of convection and cloud systems [*Randall et al.*, 2003; *Stevens and Bony*, 2013; *Schneider et al.*, 2017].

The uncertainty surrounding clouds and moist convection includes how they interact with their environment, and improving our understanding of coupling between clouds and large-scale circulations has been identified as one of climate science's "grand challenges" [*Bony et al.*, 2015]. Large-scale circulation cells are the main control on the spatial distribution of cloud types in the tropics, as deep convective clouds are found in the rising branches of the Walker and Hadley circulations, and low clouds in the marine boundary layers beneath the descending branches. But the strengths and spatial structures of these circulation cells are strongly influenced by convective transports of heat, moisture and momentum, by the release of latent heat in moist convection, and by the reflection, absorption and emission of radiation by clouds. A better understanding of the two-way interactions between clouds and large-scale atmospheric flows is needed to explain observed circulation patterns and cloud distributions, and to predict how these will change in a warmer world.

Untangling the interactions between clouds and circulation cells requires modeling set-ups that can resolve cloud-scale processes, while also representing the features that drive the circulations. For example, some representation of the zonal sea-surface temperature (SST) gradient across the tropical Pacific [or, to ensure the system is energetically closed, of the ocean heat transport associated with it; *Merlis and Schneider*, 2011] is required to study the coupling between clouds and the Walker circulation. Similarly, setting up a Hadley circulation requires rotation and meridional surface temperature gradients.

A number of recent studies have documented how clouds in global climate models (GCMs) respond to changing SST patterns, setting aside the question of how large-scale circulations mediate these responses. Past studies have examined how clouds respond to the oscillations of the zonal SST gradient in the equatorial Pacific during the El Niño-Southern Oscillation (ENSO) cycle [e.g., *Park and Leovy*, 2004; *Lloyd et al.*, 2012; *Radley et al.*, 2014; *Lutsko*, 2018; *Middlemas et al.*, 2019; *Ceppi and Fueglistaler*, 2021] and how changing SST patterns induce variations in the net climate feedback through their effects on cloud distributions. The latter includes studies of changing SST and cloud cover patterns over the historical period [*Andrews et al.*, 2018; *Silvers et al.*, 2018; *Dong et al.*, 2021; *Andrews et al.*, 2022], and of the "pattern effect", whereby the evolution of SST patterns causes cloud feedbacks to vary over time, even if CO_2 concentrations are held fixed after an initial step increase [e.g., *Armour et al.*, 2013; *Meraner et al.*, 2013; *Andrews et al.*, 2015; *Stevens et al.*, 2016; *Ceppi and Gregory*, 2017; *Andrews and Webb*, 2018; *Dong et al.*, 2020]. A related set of studies have calculated Green's functions for the response of the cloud radiative effect to localized SST anomaly patches [*Zhou et al.*, 2017; *Dong et al.*, 2019]. Together, these different lines of investigation have shown that perturbing SSTs in the tropical west Pacific induces large non-local cloud changes, which affect global climate through the top-of-atmosphere radiation budget. Conversely, perturbations in the tropical east Pacific tend to produce a more localized response [see also *Bloch-Johnson et al.*, 2020]. However, the dynamical mechanisms linking specific SST perturbations to their cloud responses have yet to be investigated in depth, partly because of the lack of idealized modelling set-ups which capture the relevant dynamics.

In this study, we examine the potential for "mock-Walker" simulations to help address these issues. Mock-Walker simulations use convection-permitting models (CPMs, also often called cloud-resolving models) in long-channel rectangular domains, with SSTs varying in the long dimension. Hence they include the zonal SST gradient needed to generate a realistic Walker-like circulation, while using grid resolutions sufficient to partially resolve convective processes. The mock-Walker set-up was first introduced by *Grabowski et al.* [2000], and we briefly review the subsequent literature in the following subsection. Here, our goals are to assess how well mock-Walker simulations can reproduce the observed climate of the tropical Pacific, to describe their responses to surface warming and to provide insight into the dynamics of the circulation in this modeling set-up. We focus in particular on the transition from a single-celled to a double-celled overturning circulation as the mean SST of mock-

Walker simulations is increased. Described in more detail below, the transition dominates the response of mock-Walker simulations to warming and, since double-cells appear to be less prevalent in the real tropical atmosphere, complicates the utility of the mock-Walker set-up for studying cloud feedbacks. The prominence of double-celled circulations is both a note of caution for studies of mock-Walker simulations, and something that merits further attention to determine whether it could occur in the real world.

In addition to potentially acting as a useful modelling framework for studying the interactions between SST perturbations, large-scale circulations and convection, we believe that mock-Walker simulations can act as a bridge between small-domain (widths of O(100 to 100s km)) CPM studies and the observed tropical atmosphere. Small-domain CPM simulations have provided many insights into the behavior of the tropical atmosphere and its response to warming [e.g., *Muller et al.*, 2011; *Muller and Held*, 2012; *Singh and O'Gorman*, 2013; *Romps*, 2014; *Wing and Emanuel*, 2014; *Seeley and Romps*, 2015; *Harrop and Hartmann*, 2016; *Hartmann et al.*, 2019; *Abbott et al.*, 2020]; however, directly relating results from small-domain CPM simulations to the real tropical atmosphere is often complicated because the simulations are run over horizontally uniform SSTs, and do not generate large-scale flows.

Convection in CPM simulations also tends to cluster in a portion of the domain – a phenomenon known as convective self-aggregation [see *Wing*, 2019, for a recent review]. Convective self-aggregation is sensitive to the details of the model set-up and typically occurs for larger domains and coarser grids, so simulations run under slightly different conditions can produce very different climates [*Wing et al.*, 2018a]. Global simulations of radiative-convective equilibrium (RCE), with parameterized clouds and convection, also exhibit self-aggregation [e.g., *Arnold and Randall*, 2015; *Coppin and Bony*, 2015; *Reed et al.*, 2015; *Pendergrass et al.*, 2016]. The mock-Walker set-up forces convection to cluster over the warmest SSTs[1], so there is less ambiguity about interpreting aggregation and about how simulations relate to the real tropical atmosphere; mock-Walker simulations can thus be viewed as a complement to small-domain RCE simulations.

[1] As an alternative, *Popp and Bony* [2019] and *Popp et al.* [2020] forced the convection in their global aquaplanet simulations to organize over patches of enhanced evaporation.

We begin by briefly reviewing previous mock-Walker studies in the following subsection, then describe the model and simulations we have performed in section 2. We compare the climates of a set of mock-Walker simulations to the observed atmosphere over the tropical Pacific in section 3, before examining the response of the mock-Walker set-ups to uniform warming in section 4. In section 5 we discuss the transition to a double-cell circulation seen in our simulations and in other studies. Radiative-subsidence provides a useful diagnostic of the transition, but sharp variations in stability and humidity make it difficult to determine a priori whether a given SST distribution will support a multi-celled overturning circulation. Finally, we end with conclusions in section 6.

1.1 Previous mock-Walker studies

Past studies of mock-Walker simulations have generally fallen into three categories: *(1)* investigations of the mean states of mock-Walker simulations, *(2)* investigations of the variability of mock-Walker simulations, and *(3)* comparisons of mock-Walker simulations with simpler models.

Mean states of mock-Walker simulations

To our knowledge, the first study of mock-Walker simulations was by *Grabowski et al.* [2000], who found that 2D mock-Walker simulations with interactive radiation developed two vertically-stacked overturning cells (i.e., with two separate detached maxima in the longitude-height overturning streamfunction). We will refer to this as as a “double-celled circulation” or a “double cell” for short. *Grabowski et al.* [2000] showed that the double cells in their simulations could be eliminated by prescribing a fixed radiative cooling profile or by horizontally homogenizing radiative heating rates throughout the domain.

In follow-up work, *Yano et al.* [2002a] diagnosed the balances controlling the mean states of these circulations, and emphasized the importance of the vertical structure of convective heating in determining formation of a single or double cell. Although this is relevant for interpreting the large-scale flow in our simulations, we have sought an explanation that requires no knowledge of the vertical structure of convective heating (*Iipponen and Donner* [2020] derived analytic solutions for Walker Circulations driven by idealized convective heating profiles, but did not compare these solutions with mock-Walker simulations). In a later study, *Liu and Moncrieff* [2008] examined the roles of surface friction, SST gradients, and horizontal contrasts in radiative cooling in regulating convection and circulation in mock-Walker simulations. A key result was that other factors besides SST gradients play important roles in determining the strength of the surface winds, which connect to the location and strength of convection – in contrast to the classical picture of *Lindzen and Nigam* [1987].

Finally, *Silvers and Robinson* [2021] compared mock-Walker simulations with horizontal grid-spacings ranging from 1km to 100km, with and without parameterized convection. These span the range from CPM simulations, as performed here, to mock-Walker simulations at GCM resolutions. Key findings include that coarser resolution simulations produce fewer upper-level clouds, more low-level clouds, weaker overturning circulations, and more precipitation. In general, the simulated cloud cover in the GCM-resolution simulations resembled observed cloud cover more closely than the finer resolution simulations, suggesting that the GCM's cloud and convection schemes have been tuned to observations. Additional experiments were performed in which the longwave (LW) cloud radiative effect (CRE) was disabled, but the effects of doing this were sensitive to resolution.

Variability of mock-Walker simulations

In another follow-up to the *Grabowski et al.* [2000] study, *Yano et al.* [2002b] performed a linear perturbation analysis to understand the variability of mock-Walker simulations. This analysis suggests that Walker circulations are linearly unstable, and spontaneously generate convectively-coupled gravity waves. Several other studies have noted that convectively-coupled waves cause quasi-periodic oscillations in mock-Walker simulations, corresponding to expansions and contractions of the convecting region. These oscillations generally occur on time-scales of ~2 days [*Grabowski et al.*, 2000; *Bretherton et al.*, 2006], though *Slawinska et al.* [2014] found longer time-scales of ~20 days. By analyzing specific events, *Slawinska et al.* [2014] showed that – in their set-up – the ~20-day variability is related to synoptic-scale systems, and that expansions and contractions of the convecting region involve different dynamics. The longer time-scales in their simulations are due to the use of a much larger domain: roughly 40,000km in the long dimension versus roughly 4000km in the other studies.

Comparisons with simpler models

Bretherton et al. [2006] compared CPM mock-Walker simulations with the Simplified Quasi-equilibrium Tropical Circulation Model (SQTCM), an idealized model of the tropical atmosphere based on quasi-equilibrium theory that includes simplified representations of cumulus convection and cloud-radiative feedbacks. The SQTCM was able to produce reasonable representations of the horizontal distributions of rainfall and horizontal energy fluxes in the mock-Walker simulations, however it was not able to capture the humidity distribution, the vertical structure of the circulation or the circulation's scaling with domain-size. *Kuang* [2012] mimicked the behavior of weakly-forced (i.e., weak SST gradient) mock-Walker simulations by combining linear response functions (to represent the cumulus ensemble) with a parameterization of the large-scale flow based on the gravity wave equation. This simplified system could reproduce the behavior of simulations with organized convection, including their sensitivity to moisture and temperature perturbations, but performed poorly as the convection became more disorganized. *Wofsy and Kuang* [2012] compared horizontal precipitation and latent heating distributions in 2D mock-Walker simulations with prescribed radiative cooling to a modified form of the theoretical Walker circulation model of *Peters and Bretherton* [2005]. An important modification by *Wofsy and Kuang* [2012] was the addition of a gustiness parameter, which allowed the theoretical model to capture the narrowing of the warm pool as the radiative cooling was strengthened.

Other studies

In addition to these three categories of mock-Walker studies, the most similar previous study to the present work is *Larson and Hartmann* [2003], who compared the climate of mock-Walker simulations run using the fifth-generation Pennsylvania State University-National Center for Atmospheric Research (PSU/NCAR) Mesoscale Model (MM5) with observations of the tropical Pacific, and also investigated the model's response to warming and to changing SST gradients. The MM5 model produced a reasonable simulation of the observed circulation, though it also produced a double-cell circulation. Increasing the SST gradient resulted in a more intense circulation and a narrowing of the convecting region, while increasing the mean SST but keeping the gradient fixed weakened the circulation slightly. Surprisingly, the outgoing longwave radiation (OLR) was found to be roughly insensitive to the SST changes, because of compensating positive and negative feedbacks, whereas the shortwave (SW) radiation was found to be highly sensitive to SST changes, due to the model's low cloud response. However, the finest grid-spacing used by *Larson and Hartmann* [2003] was 60km – far too coarse to resolve cloud processes. We also used 2D mock-Walker simulations as part of an investigation of the changes in precipitation efficiency with warming, finding that the precipitation efficiency is high in regions of deep convection and low in the stratus clouds over the cold pool [*Lutsko and Cronin*, 2018].

Finally, a number of studies have performed RCE simulations in domain geometries akin to mock-Walker set-ups, but over uniform SSTs, to explore mechanisms that lead to organization of convection, the strength of large-scale circulations, and how cloud and rain distributions change with warming [*Grabowski and Moncrieff*, 2001, 2002; *Stephens et al.*, 2008; *Posselt et al.*, 2008, 2012; *Wing and Cronin*, 2016; *Cronin and Wing*, 2017]. The RCEMIP project also included an "RCE_large" set-up, consisting of a rectangular channel with a 16:1 aspect ratio and uniform SSTs [*Wing et al.*, 2018b, 2020]. Although the large-scale circulations in these simulations are far less constrained than in mock-Walker simulations, certain properties of observed large-scale tropical flows can be reasonably reproduced, such as the distributions of large-scale mid-tropospheric vertical motion [*Cronin and Wing*, 2017] and humidity variability [*Holloway et al.*, 2017], as well as the diabatic processes that favor and disfavor convective aggregation over a range of length scales [*Beucler et al.*, 2019]. These uniform-SST long-channel simulations provide another useful stepping stone for relating small domain CPM studies to the observed tropical atmosphere [see also *Wing et al.*, 2018a].

2 Model, Simulations and Data

2.1 Model description

All simulations were performed with version 6.10.8 of the System for Atmospheric Modeling (SAM, *Khairoutdinov and Randall* [2003]). This model solves the anelastic continuity, momentum and tracer conservation equations, and its prognostic thermodynamic variables are liquid/ice water static energy, total nonprecipitating water (vapor, cloud water and cloud ice) and total precipitating water (rain, snow and graupel).

The simulations were conducted without rotation and with fixed SSTs, and used a vertical grid with 64 levels, starting at 25m and extending up to 27km. The vertical grid spacing increases from 50m at the lowest levels to roughly 1km at the top of the domain. A sponge layer damps the flow at the top of the domain, and subgrid-scale fluxes are parameterized using Smagorinsky's eddy diffusivity model. A variable time-step was used, with maximum interval 10s, and radiative fluxes were calculated every 40 time-steps. The incoming solar radiation was fixed at 650.83Wm^{-2}, with a zenith angle of 50.5° [*Tompkins and Craig*, 1998], producing a net insolation close to the tropical-mean value. The simulations were initialized with a small amount of white noise added to the temperature field near the surface to initiate convection. All simulations used the single-moment SAM microphysics scheme [*Khairoutdinov and Randall*, 2003] and the CAM radiation scheme [*Collins et al.*, 2006].

2.2 Simulations

We focus on 3D simulations conducted in a domain of length $L = 12{,}288$km in the x-direction and width 96km in the y-direction. SSTs are prescribed to a profile that is sinusoidal in x, with a wavelength of $2L$ such that the SST varies over half a wavelength within the domain, and a peak-trough amplitude of ΔT: $\mathrm{SST}(x) = T_0 + \frac{\Delta T}{2}\cos(\pi x/L)$. The domain is periodic in y, but bounded by rigid walls at $x = 0$ and $x = L$, with the warmest SSTs located near one wall and the coldest SSTs near the other wall. The horizontal grid-spacing is set to 3km in all simulations. Tests showed that using a domain with walls has a minor effect on the flow in the model compared to using a doubly-periodic domain of length $2L = 24{,}576$km, which would allow the SST to vary over a full wavelength, with primary differences localized to within about 100km of the walls (not shown). We used smaller domains with walls in order to reduce computational burden. All simulations were run for 200 model days, with averages taken over the last 100 days.

Our comparison with observations focuses on three simulations, run with mean SST $T_0 = 300.5$K and with ΔT values of of 4K, 5K and 6K (see Figure 1). We will refer to these simulations as the "El Niño", "control" and "La Niña" simulations, respectively. We have also run three warming simulations, in which the SSTs in each set-up are uniformly warmed by 2K (i.e., $T_0 = 302.5$K), as well as a strong cooling simulation ($T_0 = 290$K) and a strong warming simulation ($T_0 = 310$K), with ΔT set to 5K in both cases. A complete list of the 3D simulations is given in Table 1.

2.3 Reanalysis and observational data

Monthly-mean meteorological data are taken from the ERA5 dataset [*Hersbach et al.*, 2020] and monthly-mean top-of-atmosphere (TOA) radiative fluxes from the Clouds and the

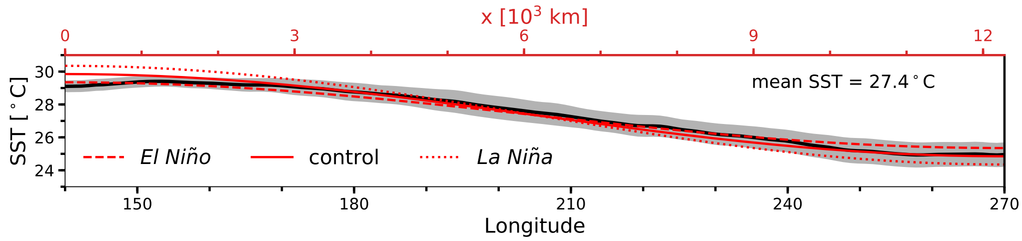

Figure 1. Climatological SSTs, averaged from 5°S to 5°N, in the equatorial Pacific. The black line shows the mean SST at each longitude and the shading shows ±1 standard deviation. Data are taken from the HADISST1 dataset, available from https://www.metoffice.gov.uk/hadobs/hadisst/, and span the period 1950-2017. The regional-mean sea surface temperature is 27.4°C. The dashed, solid and dotted red lines show the SST profiles in the El Niño, control and La Niña mock-Walker simulations, respectively. The bottom x-axis corresponds to the HADISST data, and spans a distance of roughly 14,430km, while the top x-axis corresponds to the SAM domain and spans 12,288km; i.e., the bottom axis is stretched by ~17% compared to the top axis.

Table 1. List of 3D mock-Walker simulations performed with SAM.

simulation name	T_0 [K]	ΔT [K]
control	300.5	5
El Niño	300.5	4
La Niña	300.5	6
+2K warming	302.5	5
+2K warming-El Niño	302.5	4
+2K warming-La Niña	302.5	6
strong cooling	290	5
strong warming	310	5

Earth's Radiant Energy System (CERES) dataset. We have used ERA5 data for the period 1979-2020, and subsampled the data their native 0.25° × 0.25° grid to a 1° × 1° grid. The CERES data comprise all-sky and clear-sky TOA fluxes, from which we have calculated the cloud radiative effect (CRE) as all-sky fluxes minus clear-sky fluxes. Data are taken for the period March 3rd 2003 to October 10th 2013, and interpolated onto a 1° × 1° grid.

We consider the atmosphere above a section of the equatorial Pacific, from 140°E to 270°E and meridionally-averaged from 5°S to 5°N. This is comparable to the length of the mock-Walker domain (~14,430km compared to 12,288km) and includes both a maximum and a minimum in the climatological SST profile (Figure 1). There is some ambiguity as to which latitude band is most appropriate for modeling the Walker circulation in the absence of realistic meridional SST gradients, so we have also compared with other latitude bands (15°S–5°S, 10°S–0°, 0°–10°N and 5°N–15°N), but the results of the comparisons with the mock-Walker simulations are qualitatively unchanged.

3 Comparing the Mock-Walker Simulations with Observations

3.1 Warm pool and cold pool climates

We begin by comparing the climates of the "warm pool" and "cold pool" regions of the simulations with observations over the West and East Pacific, respectively. Figure 2 shows vertical profiles of temperature, relative humidity, moist static energy (MSE = $c_p T + L_v q_v + gz$)[2] and vertical pressure velocity from reanalysis (black lines) and the simulations (cyan, blue and magenta lines). The top panels show averages taken over the warm pools (150-170°E and 5°S-5°N in reanalysis and x = 1-3×10^{3}km in the simulations, see the solid white bars in Figure 4), and the bottom panels show averages taken over the cold pools (240-260°E and 5°S-5°N in reanalysis and x = 10-12×10^{3}km in the simulation, see the dashed white bars in Figure 4).

Warm-pool profiles compare much more tightly between the simulations and reanalysis than do cold-pool profiles. Over the warm pools, simulated temperature profiles closely match reanalysis (Figure 2a), though there is a notable difference between the boundary layer and the free troposphere. Below about 950hPa, the differences between the simulated

[2] c_p is the heat capacity of dry air, T is temperature, L_v is the latent heat of vaporization of water, q_v is specific humidity, g is Earth's gravitational acceleration and z is height

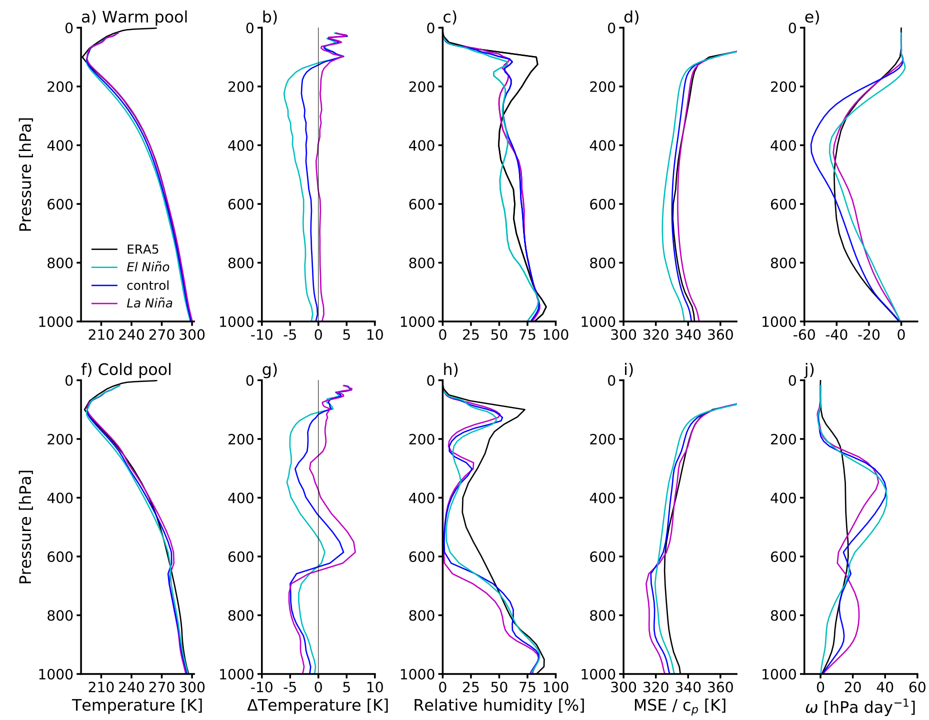

Figure 2. a) Vertical profiles of temperature in the warm pool of the ERA5 data (solid black) and in the warm pool regions of the El Niño, control and La Niña simulations (solid, dashed and dotted blue lines, respectively). b) Warm pool temperature differences between the three simulations and the climatological ERA5 data. The simulation data are linearly interpolated onto the reanalysis grid. c) Same as a), but showing vertical profiles of relative humidity, averaged over the same regions. d) Same as a), but showing vertical profiles of moist static energy, averaged over the same regions. e) Same as a), but showing vertical profiles of the vertical pressure velocity, averaged over the same regions. f) Vertical profiles of temperature in the cold pool of the ERA5 data (solid black) and in the cold pool regions of the El Niño, control and La Niña simulations (solid, dashed and dotted blue lines, respectively). g) Same as panel b), but for cold pool temperature profiles. h) Same as f), but showing vertical profiles of relative humidity, averaged over the same regions. i) Same as f), but showing vertical profiles of moist static energy, averaged over the same regions. j) Same as f), but showing vertical profiles of the vertical pressure velocity, averaged over the same regions.

temperatures and the reanalysis temperatures follow the warm pool SSTs (Figure 2b): the El Niño simulation is slightly cooler and the La Niña simulation slightly warmer. Above 950hPa the simulated warm pools are relatively cooler compared to reanalysis; e.g., the control temperatures, which are very similar near the surface, are colder than reanalysis above the boundary layer, with the gap increasing with height and peaking near 200hPa. The El

Niño simulation is even colder, while the La Niña temperatures are very similar to the reanalysis above the boundary layer, despite the warmer surface temperatures.

The simulated warm pool relative humidities (Figure 2c[3]) and MSE profiles (Figure 2d) are generally similar to the ERA5 data. The warm pool MSE is notably lower in the El Niño simulation, which reflects colder temperatures and lower relative humidities in the mid-troposphere. The ascent velocities are comparable, but tend to be more top-heavy in the simulations (Figure 2e). In reanalysis data, the vertical velocity peaks at around 500hPa, with faster ascent in the lower troposphere than in any of the simulations.

Over the cold pools, simulated thermodynamic and dynamic profiles differ much more from the ERA5 data. The simulations are substantially colder in the lower troposphere, and all three have strong temperature inversions at about 650hPa that are not seen in the reanalysis (Figure 2f; note that the simulated cold pools also have boundary layer-capping inversions near 900hPa). Figure 2g shows the simulated cold pool temperatures are substantially colder than reanalysis near the surface, further suggestive of issues with SAM's boundary layer scheme (or surface flux parameterizations). The simulated cold pools are drier than the reanalysis data at almost all levels, with the relative humidities approaching 0% in the mid-troposphere (Figure 2h). Reflecting these differences, the MSE is 20-25K lower in the lower troposphere of the simulations than in reanalysis (Figure 2i). Above the inversions the simulated MSE values are closer to the observed MSE profile, but remain generally lower than observed. In all three simulations, the descent profiles over the cold pools have much larger magnitudes than reanalysis (Figure 2j); we hypothesize these fast descent speeds occur because the simulated domain is closed, so mass must be conserved, whereas the reanalysis data are averaged over an open domain at latitudes of mean ascent. The La Niña and control profiles also have two distinct descent maxima, one in the upper troposphere and one in the lower troposphere. The implied double-celled flow structures are discussed more below.

Simple models of the Walker circulation often represent ascent and descent with a single vertical mode [the first baroclinic mode, e.g., *Bretherton and Sobel*, 2002; *Peters and Bretherton*, 2005; *Wofsy and Kuang*, 2012; *Emanuel*, 2019]. That the ascent in the warm

[3] By default, SAM outputs relative humidity calculated over liquid water only, but we report relative humidities over liquid water for temperatures ≥0°C and over ice for temperatures <0°C. Equation 7 from *Murphy and Koop* [2005] is used to calculate the saturation vapor pressure over ice.

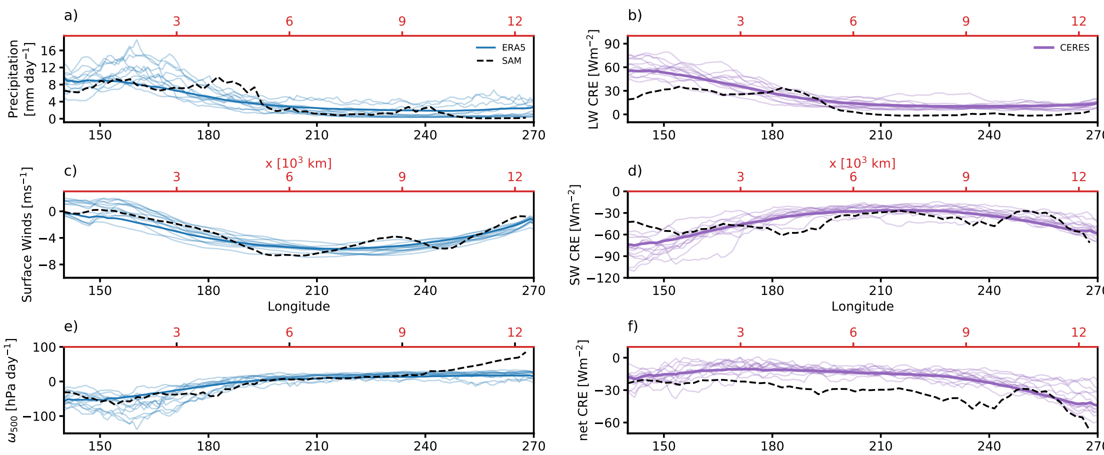

Figure 3. a) Climatological precipitation over the equatorial Pacific, averaged from 5°S to 5°N, for the ERA5 data (thick blue line) and precipitation averaged over the last 100 days of the control 3D SAM simulation (dashed red line). The thinner blue lines show monthly-means of equatorial Pacific precipitation for the year 2006, which was a neutral ENSO year. b) Climatological LW CRE over the equatorial Pacific, averaged from 5°S to 5°N, for the CERES data (thick purple line) and LW CRE averaged over the last 100 days of the control 3D SAM simulation (dashed red line). The thinner purple lines show monthly-mean LW CRE for the year 2006. c) Same as a) but for the near-surface zonal winds. d) Same as b) but for the SW CRE. e) Same as a) but for the ω_{500} velocities. f) Same as b) but for the net CRE. Note that in all panels the scale of the bottom x-axis corresponds to the reanalysis and satellite data, while the scale of the top x-axis corresponds to the SAM domain.

pool regions exhibits a single maximum and the descent in the cold pool regions exhibits two maxima suggests that such simple theories will not capture the behavior of our simulations. Furthermore, the large differences in the MSE profiles across the domains suggest that energy transports cannot be diagnosed solely from vertical velocity profiles [e.g., *Back and Bretherton*, 2006; *Inoue and Back*, 2015]. Thus, a full theory for the circulation and energy transport in this mock-Walker set-up must consider at least two modes of variability in vertical velocity, horizontal advection across MSE gradients, and substantial variation of the temperature and humidity profiles between warm-pool and cold-pool regions.

3.2 Zonal profiles

Next, we compare zonal profiles of meteorological variables and cloud radiative effects (CREs) from the mock-Walker simulations with reanalysis and satellite data. The CRE comparison is of particular interest, since one of our primary aims is to assess the utility of the mock-Walker set-up for studying cloud feedbacks under warming. For ease of presentation, we will only show values for the control mock-Walker simulation, but note that the main differences with the satellite observations and reanalysis data are seen in all the 300K simulations.

There are a number of similarities between the control simulation and the ERA5 data. The maximum precipitation in the simulation is comparable to the reanalysis data, though the sharp simulated transition from high to low precipitation rates resembles individual observed months more than the long-term ERA5 climatology (Figure 3a). A secondary simulated peak in precipitation near $x = 9{\times}10^3$km is not seen in observations. Simulated surface winds compare closely in magnitude and overall shape to reanalysis winds, but show more than one local maximum in speed, in contrast to the reanalysis data (Figure 3c). Higher up, the simulated ω_{500} compares well to the reanalysis except over the far-eastern cold pool where the simulated descent is far stronger (see also Figure 2h).

The simulated LW CRE shows broadly similar structure to the CERES climatology in that both are stronger over the warm pool and weaker over the cold pool (Figure 3b), but the magnitude of simulated LW CRE averages only half that seen in observations. The SW CREs in CERES observations and the control simulation have comparable magnitudes (Figure 3d), but the simulated SW CRE shows additional minima near the precipitation maxima at $x = 4 \times 10^3$km and $x = 9 \times 10^3$km, as well as near the eastern boundary of the domain. As with precipitation, the more jagged simulated SW CRE profile compares better with monthly observations than with climatology, but even on monthly time-scales the simulated LW CRE is biased low.

These discrepancies in the LW and SW CRE lead to substantial differences in the net CRE profiles between simulations and observations (Figure 3f): net CRE is biased low across most of the middle of the domain and over the eastern boundary by $\sim$ 20 Wm^{-2}. We note, however, that the simulated SW CRE may be overestimated in magnitude, as SAM uses a daytime-weighted zenith angle, rather than an insolation-weighted zenith angle [*Cronin*, 2014]. With a global-mean cloudscape, this would give an overestimate of the SW CRE's magnitude of about 10 Wm^{-2}, and would partly compensate for the bias in the net CRE.

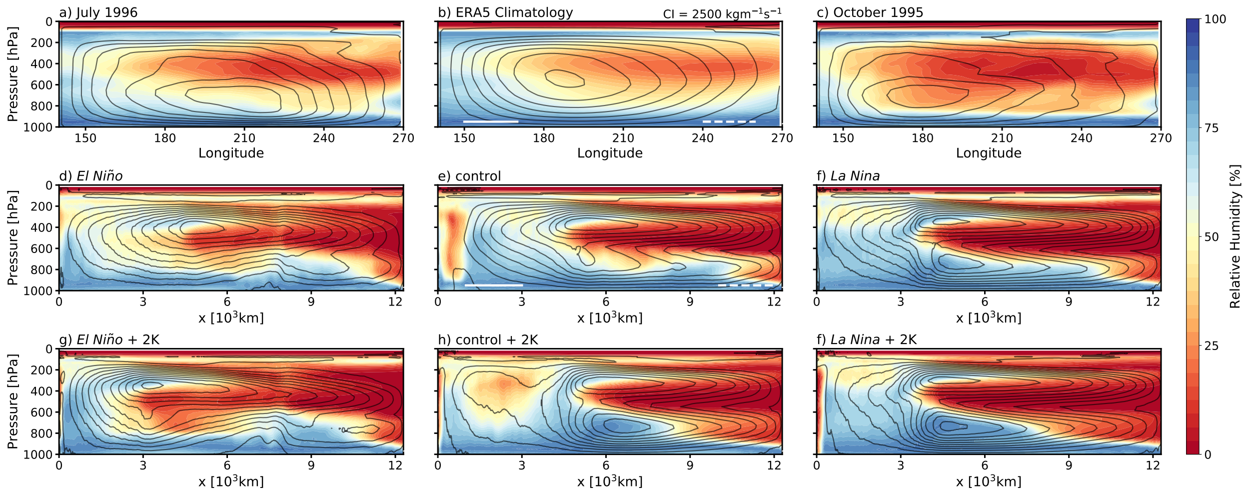

Figure 4. a) Relative humidity (colored contours) and streamfunction (black contours) for June 1996. b) Same as panel a) but showing climatological values. c) Same as panel a) but for October 1995, one of the driest months over the eastern Pacific in the ERA5 record. d) Mean relative humidity (colored contours) and streamfunction (black contours) in the El Ni SAM simulation. e) Same as panel d) but for the control SAM simulation. f) Same as panel d) but for the La Niña SAM simulation. g) Same as panel d) but for the +2K El Niño SAM simulation. h) Same as panel d) but for the +2K control SAM simulation. i) Same as panel d) but for the +2K La Niña SAM simulation. The contour interval for the streamfunctions is the same in all panels, with solid contours indicating clockwise flow and dashed contours indicating counterclockwise flow. The solid white and dashed white lines in panels b and e indicate the warm pool and cold pool regions, respectively, in the reanalysis data and in the simulations.

3.3 Overturning circulation

Finally, we compare the simulated and observed overturning circulations. The top two rows of Figure 4 show the streamfunctions (black contours) and the relative humidities (colored contours) for June 1996 (panel a); for the climatological ERA5 data (panel b); for October 1995 (panel c); and for the three simulations (panels d-f). October 1995 is one of the driest months over the east Pacific in the ERA5 record, while June 1996 was more typical of monthly conditions over the tropical Pacific. The streamfunctions are calculated in the mock-Walker simulations as $\int_{\phi_0}^{\phi} \omega(p,\phi')d\phi'$, where ω is the meridionally-averaged vertical pressure velocity, p is pressure and ϕ is longitude, and in the reanalysis data as $\int_{\phi_0}^{\phi}(\omega(p,\phi') - \bar{\omega}(p))d\phi'$, where the overbar denotes a zonal average over the region 140° to 270°E and ω is averaged over 5°S-5°N. Since the reanalysis data are averaged over a limited sector, the corresponding streamfunctions do not conserve mass, and we subtract the sectoral mean in order to remove the influence of the zonal-mean ascent at these latitudes.

Flows in the six panels have some broad similarities – ascent over the warm pool (the West Pacific), outflow in the upper troposphere, descent over the cold pool (the East Pacific) and a decrease in the upper tropospheric relative humidity moving eastward from the warm pool to the cold pool[4] – but several important differences are also apparent. First, the simulated mid- and upper-tropospheres are much drier than the reanalysis over the cold pool, with minimum relative humidities close to 0%, compared to a minimum relative humidity of ~30% in the ERA5 climatology. In October 1995 there was a dry patch with a minimum relative humidity of ~5%, but we have been unable to find a month in which the relative humidity minimum approached 0%, suggesting that transient tropical waves or meridional moisture transports not simulated by the model play a crucial role in moistening the middle and upper troposphere over the cold pool.

A second major difference is that the flow in the SAM simulations tends to exhibit a double-celled structure, particularly over the cold pool. The double-cell is most clearly defined in the La Niña simulation and least defined in the El Niño simulation, but even in this case there is a secondary circulation cell in the lower troposphere over the cold pool. The existence of the double cells is also evident from the presence of two descent maxima in all three simulations (Figure 2h). That the La Niña simulation exhibits the most well-defined double cell suggests that either stronger zonal temperature gradients or warmer warm pool temperatures promote the development of a double-celled circulation.

By contrast, the reanalysis tends to show a single overturning cell in both climatology and individual months. The circulation does hint at a double cell in October 1995, suggesting a link between tropospheric relative humidity and flow structure, but we have been unable to find any months which exhibit as clear double cells as are seen in the simulations. (Note that *Zhang and McGauley* [2004] and subsequent studies have demonstrated the existence of a shallow meridional circulation in the tropical east Pacific.)

[4] We are unsure what causes the dry quiescent region over the western edge of the warm pool in the control SAM simulation. It may be a transient feature, which would be smoothed out in longer simulations, or it could be caused by the presence of a wall in our simulations or the lack of background zonal flow, though these seem unlikely as this feature is not present in the other simulations.

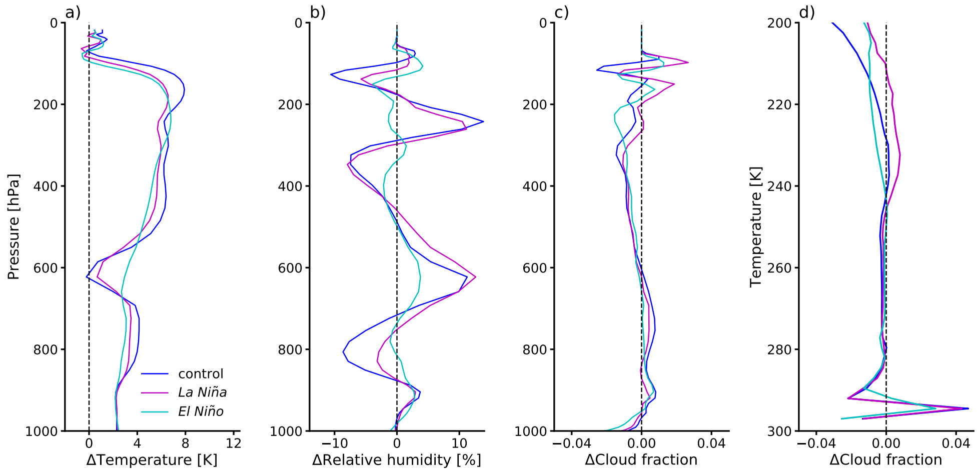

Figure 5. a) Response of horizontal-mean temperature to increasing the mean SST by 2K with the control SST gradient (black curve), with the enhanced La Niña gradient (blue curve) and with the reduced La Niña gradient (red curve). b) Same as a) but for the relative humidity. c) Same as a) but for the cloud fraction. d) Same as c) but with the cloud fraction changes plotted versus temperature instead of pressure.

4 Responses to Increasing Mean SST

We have run simulations with mean SSTs ranging from 290K to 310K, but focus here on the mock-Walker response to +2K warming, which is comparable to the warming the tropical Pacific might experience under a doubling of atmospheric CO_2 concentrations. Our simulations could also be used to probe the effects of nonuniform warming; e.g., by comparing the control case with the +2K La Niña case.

Circulation changes largely govern the responses in the +2K experiments with the control and La Niña SST gradients. In both setups, the lower circulation cell expands vertically, so that the outflow is at higher altitudes (panels h and i of Figure 4), and the outflow also strengthens. In the control +2K experiment the lower cell expands horizontally, so that it spans most of the domain, instead of the more localized circulation seen in the original control experiment. The convection over the warm pool intensifies in both simulations, and also moves away from the warm pool, maximizing near $x = 5 \times 10^3$km, in the control simulation. By contrast, the circulation changes are more muted in the El Niño simulations (panel g of Figure 4f), though the upper troposphere over the cold pool is drier, suggesting a contraction of the convection (and hence less detrainment moistening) that is difficult to see in Figure 4g.

Figure 5 shows the horizontal-mean responses of temperature, relative humidity and cloud cover. The responses with the control and La Niña gradients are generally similar, while the responses for the El Niño case are weaker and show different vertical structures (panel a). In the control and La Niña simulations the vertical expansion of the lower circulation cells creates a sharp warming minimum near 600hPa in both simulations, representing the upward shift of the temperature inversion over the cold pool. The La Niña case warms more than the control case, suggesting that tropospheric warming is larger for more organized states. The warming in the +2K-El Niño simulation shows less evidence of circulation changes, and resembles warming of a moist adiabat, with a maximum near 250hPa.

In all three cases, the boundary layer relative humidity increases (panel b of Figure 5), and above this there are alternating regions of moistening and drying, again following the circulation changes. For instance, the relative humidity increases between 700hPa and 500hPa in the control and La Niña cases, as the outflow of moist air from the convecting region at the top of the lower circulation cell moves to higher altitudes. The vertical structure of the relative humidity changes in the El Niño case is similar to the control and La Niña cases, but the changes are typically less than half as large.

The cloud fraction responses are plotted as a function of both height (Figure 5c) and temperature (Figure 5d), as the low clouds (≤850hPa) stay at roughly the same height while the mid- and upper-tropospheric clouds stay fixed at roughly constant temperature, consistent with FAT/FiTT scaling [*Hartmann and Larson*, 2002; *Seeley et al.*, 2019]. Low cloud cover increases between roughly 950-900hPa and decreases closer to the surface with warming in all three set-ups, while the high cloud fraction decreases in the +2K-El Niño and +2K-La Niña simulations, but increases for the +2K control case (Figure 5d). We do not understand the reason for this difference well, but note again that the region of maximum ascent moves towards the center of the domain in the control simulation (Figure 4), so there is greater moistening of the upper troposphere by anvil detrainment. The high cloud reduction in the +2K El Niño simulation is consistent with the contraction of the convecting region noted above.

4.1 Feedbacks and Cloud Responses

A goal of this study is to assess the value of mock-Walker simulations for studying cloud feedbacks. To this end, Table 2 lists the TOA fluxes and climate feedbacks (λ) for the

Table 2. TOA fluxes and climate feedbacks in the six experiments with T_0 = 300.5K and T_0 = 302.5K. Positive fluxes denote downward radiation. The feedbacks are calculated following *Cess and Potter* [1988] as the change in net top-of-atmosphere radiation divided by 2K and uncertainties represent 5-95% confidence intervals, calculated using the standard error of the difference in daily-mean fluxes and with the number of degrees of freedom reduced to account for temporal autocorrelation.

Experiment	Net TOA flux [Wm^{-2}]	Clear-sky flux [Wm^{-2}]	CRE [Wm^{-2}]
control	56.60±0.26	87.76±0.11	-31.15±0.24
El Niño	60.68±0.22	89.08±0.09	-28.39±0.15
La Niña	53.52±0.36	85.66±0.26	-32.13±0.26
control + 2K	53.66±1.18	84.81±0.36	-31.14±0.88
El Niño + 2K	59.70±0.14	86.09±0.07	-26.39±0.12
La Niña +2K	46.55±0.73	82.62±0.85	-36.07±0.26
Response	**Net feedback [Wm^{-2}/K]**	**Clear-sky feedback [Wm^{-2}/K]**	**ΔCRE / ΔT_s [Wm^{-2}/K]**
control → control + 2K	-1.47±1.24	-1.47±0.92	0.01±0.75
El Niño → El Niño + 2K	-0.49±0.33	-1.49±0.32	1.00±0.14
La Niña → La Niña + 2K	-3.49 ±0.59	-1.51±0.71	-1.97 ±0.18
control → El Niño + 2K	+1.54±0.19	-0.83±0.13	+2.38±0.11
control → La Niña + 2K	-5.03±1.79	-2.57±1.62	-2.46±0.30

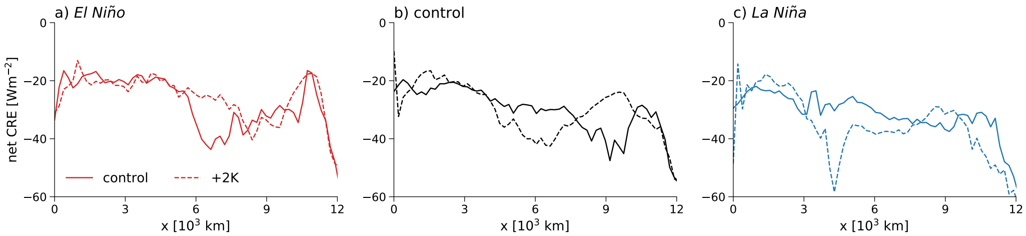

Figure 6. a) Profiles of net CRE in the El Niño mock-Walker simulation (solid curve) and the +2K El Niño simulation (dashed curve). b) Same as panel a) but for the simulations with the control SST gradient. c) Same as panel a) but for the La Niña simulations.

original and +2K experiments. λ is calculated as the change in net TOA radiative flux R between the original and +2K experiments, divided by 2K: $\lambda = \frac{R_{+2K} - R_0}{2K}$ [*Cess and Potter*, 1988], with R defined as positive for net energy input into the model. We provide net feedback and fluxes, as well as the clear-sky and CRE values.

In the original 300K experiments, the net downward TOA flux is higher for the El Niño experiment (60.68±0.22Wm^{-2}) and lower for the La Niña experiment (53.52±0.36Wm^{-2}). This inidcates both a stronger clear-sky flux in the El Niño experiment (89.08±0.09Wm^{-2}) and a weaker CRE (-28.39±0.15Wm^{-2}). We have not investigated these differences in detail, but suggest that the larger clear-sky fluxes in the El Niño case may be a result of colder tropospheric temperatures and lower outgoing longwave radiation. Although the mean SST is the same in each case, tropospheric temperatures are warmest in the La Niña case and coldest in the El Niño case, consistent with the control of free-tropospheric temperatures by convection over the warmest SSTs. Since these are warmer in the La Niña and control simulations, their upper tropospheres are warmer. The differences in CRE likely come from differences in low cloud cover, which is highest in the La Niña case and lowest in the El Niño case (not shown).

The resulting feedbacks for uniform warming are λ = -1.47±1.24 Wm^{-2}/K for the control SST gradient, λ = -3.49±0.59 Wm^{-2}/K for the enhanced La Niña gradient and λ = -0.49±0.33 Wm^{-2}/K for the reduced El Niño gradient. (Uncertainties represent 5-95% confidence intervals, calculated using the standard error of the difference in daily-mean fluxes and with the number of degrees of freedom reduced to account for temporal autocorrelation.) We have also calculated the feedback for patterned warming, e.g., increasing the zonal SST gradient (control → +2K La Niña) and decreasing the SST gradient (control → +2K El Niño).

The former gives a very strongly damping feedback of λ = -5.03±1.79 Wm^{-2}/K, while the latter leads to an unstable value of λ = +1.54±0.19 Wm^{-2}/K.

These feedback values suggests the climate sensitivity varies by a factor of ~7 across the simulations, with the El Niño set-up having a very high sensitivity (higher than any global climate model we know of) and the La Niña set-up having a very low climate sensitivity (lower than any global climate model we know of). Patterned warming can either decrease the sensitivity further (if the SST gradient is strengthened) or lead to a (locally) unstable climate state (if the SST gradient is weakened). In the latter case the instability would be coutnered by heat export to regions with net stabilizing feedbacks [*Bloch-Johnson et al.*, 2020, see, e.g.,].

In the case of uniform warming, the clear-sky feedbacks are similar across the different set-ups (Table 2), so variations in sensitivity are due to differences in the cloud feedback: the La Niña set-up has a strongly negative cloud feedback, the control set-up has a cloud feedback near zero, and the El Niño set-up has a strongly positive cloud feedback[5]. To better understand the cloud feedbacks, Figure 6 plots the net CRE profiles in the six simulations. The original El Niño profile has a strong CRE minimum over the region of shallow convection ($\sim x = 6 - 8 \times 10^3$ km, Figure 6a) which disappears with warming, suggestive of a positive feedback from reduced low cloudiness with warming. Examining Figure 5c shows that the reduction in low cloud cover occurs in the very lowest layers of the model. In the La Niña set-up, the CRE becomes more negative on the margin of the warm pool (Figure 6c), connected with both an increase in cloud fraction and cloud water paths there (not shown). This decrease in CRE features a sharp minimum at $x = 4 \times 10^3$ km, and is likely linked to changes in convection and associated high cloud cover. The net CRE also becomes more negative over the cold pool ($x = 10 - 12 \times 10^3$ km). In the control set-up, warming leads to a more negative CRE at $\sim x = 6 \times 10^3$ km), but a weakening of the negative CRE peak near $9{\times}10^3$ km; these changes compensate to produce a weak cloud feedback (Figure 6b). Comparing panels e and h of Figure 4 suggests these net CRE changes mostly come from a shift in the shallow convection towards the center of the domain.

[5] Note that for simplicity we have defined the cloud feedback as the change in CRE, which is closely related to, but not identical to, the true cloud feedback. Calculating the true cloud feedback would require estimating radiative kernels for the mock-Walker set-up.

The bottom two rows of Table 2 compare the feedbacks for patterned warming. When the SST gradient is weakened, the clear-sky feedback is almost halved compared to uniform warming, while the cloud feedback is strongly positive. When the SST gradient is strengthened the clear-sky feedback is increased by more than 50%, and the change in CRE is very strongly negative. These responses reflect differences in the original 300K simulations, though we note they are not exactly additive: taking the difference between the control and El Niño simulations, then adding $\lambda_{control}$ leads to an underestimate of the change (control → El Niño + 2K), while the same procedure overestimates the change (control → La Niña + 2K).

Although we caution against taking the feedbacks literally, the relationship we find between the SST gradient and sign of the cloud feedback – with smaller SST gradient giving a more positive cloud feedback – likely merits future investigation with mock-Walker set-ups. These results are qualitatively consistent with inferences from AMIP models forced by historical SSTs, which typically show weaker implied climate sensitivities over the past few decades, during which the SST gradient across the equatorial Pacific has been increasing [*Andrews et al.*, 2018, 2022]. They are also consistent with more idealized work on the pattern effect showing that GCM set-ups with weaker SST gradients produce weaker feedbacks and higher climate sensitivities [e.g., *Dong et al.*, 2019].

5 Discussion: The Transition to Two Vertical Cells

As mentioned in the introduction, double cell circulations have been seen in a number of previous mock-Walker studies [*Grabowski et al.*, 2000; *Yano et al.*, 2002a; *Larson and Hartmann*, 2003; *Liu and Moncrieff*, 2008; *Silvers and Robinson*, 2021]. Double-cell structures have also been found in RCE simulations over fixed SSTs [*Ruppert Jr and Hohenegger*, 2018] and in global RCE simulations over a mixed-layer ocean [*Hartmann and Dygert*, 2022]. In previous work, we found that the flow in 2D mock-Walker simulations transitions from a single vertical cell at relatively cold (<∼300K) SSTs to a double cell at warmer SSTs (>∼300K) [*Lutsko and Cronin*, 2018]. This transition is reproduced in 3D simulations (Figure 7): for a mean SST of 290K there is a single overturning cell and for a mean SST of 310K there is a clear double cell, with strong outflow from the convecting region in the mid-troposphere at around 500hPa. As in the 2D simulations, the transition seems to take place for a mean SST near 300K.

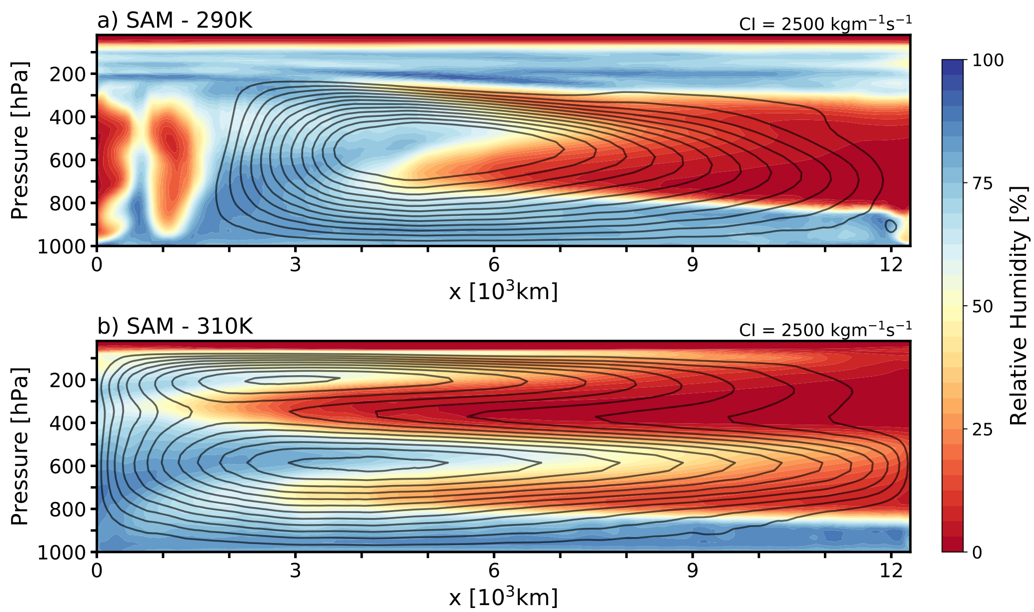

Figure 7. a) Mean relative humidity (colored contours) and streamfunction (black contours) for the SAM simulation with a mean SST of 290K. b) Same as panel a) but for the SAM simulation with a mean SST of 310K. Note that in this simulation the vertical grid had 72 levels and extended to 35km. The contour interval is the same in both panels, with solid contours indicating positive (clockwise) flow and dashed contours indicating negative flow.

In addition to the explanation by *Yano et al.* [2002a] based on convective heating profiles mentioned in section 1.1, several other mechanisms have been proposed for the development of double-celled tropical circulations, based on radiative-subsidence balance. That is, in a steady circulation, without convective heating or horizontal temperature advection, subsidence over the cold pool is constrained by the radiative cooling, Q_R, divided by the stability, S:

$$\omega_R(p) = Q_R(p)/S(p). \tag{1}$$

Grabowski et al. [2000] and *Mapes* [2001] both noted the weak stratification in the upper troposphere over the cold pool, which requires stronger subsidence to balance the radiative cooling, though *Grabowski et al.* [2000] also showed that the radiative cooling was weak in the upper troposphere over the cold pool. *Hartmann and Dygert* [2022] focused on the strong radiative cooling at the top of a lower-tropospheric moist layer, which should induce a minimum in ω_R.

We show here that ω_R qualitatively reproduces the full velocities over the cold pools of the simulations, at least above the boundary layer (dashed lines in Figure 8a[6]; note that the balance in equation 1 will break down in the boundary layer where shallow convection and horizontal advection introduce additional terms into the thermodynamic equations), and the radiative-subsidence velocities are consistent with a transition to a double-cell circulation across the 290K, control and 310K simulations. Thus a complete explanation for the development of double celled circulations at warm SSTs requires theories for the vertical structures of Q_R and S. But these are complex in our simulations: there are strong near-surface maxima in both quantities in the 290K, control and 310 simulations (panels a and b of Figure 8), and there are also strong mid-tropospheric maxima in stability and radiative cooling in the control and 310K simulations (at 650hPa and 375hPa, respectively). Comparing across the panels of Figure 8 suggests that the mid-tropospheric maxima in S and Q_R are co-located with inflow of warm, moist air into the cold pool region. We are unsure whether the horizontal inflow, and the resulting maxima in S and Q_R, cause the double cell or are a result of the double cell. We have tracked the evolution of the stability and radiative cooling over the course of these simulations, but have been unable to isolate the development of the double cell from the spin-up of the model and the large internal variability. Ensemble simulations may be needed to capture this development.

The complexity of the S and Q_R profiles, as well as the uncertainty over what initially causes the double cell to develop, make it difficult to develop simple models for ω_R. For example, the one-dimensional simple spectral model (SSM1D) of *Jeevanjee and Fueglistaler* [2020] for atmospheric radiative cooling could be combined with an assumption of moist adiabatic stratification. But SSM1D assumes fixed relative humidity and it is clear that relative humidity variations are crucial here. Incorporating variable relative humidity into the SSM1D is complicated because the radiative cooling depends on the water vapor path, and hence on the bulk relative humidity. Moreover, Figure 8c shows that the stability is far from moist adiabatic over the cold pool of these simulations: S increases with surface warming for a moist adiabatic column, but here S is essentially the same in the three simulations away from the stability maxima (e.g., compare near 600hPa of the 290K and 310K simulations). The existence of a mid-tropospheric minimum in ω_R also requires the stability maximum to

[6] Because of SAM's staggered grid, we have averaged Q_R to the interface levels and calculated S using centered difference of adjacent mass levels, such that our estimates of ω_R can be compared to ω at the appropriate interface levels

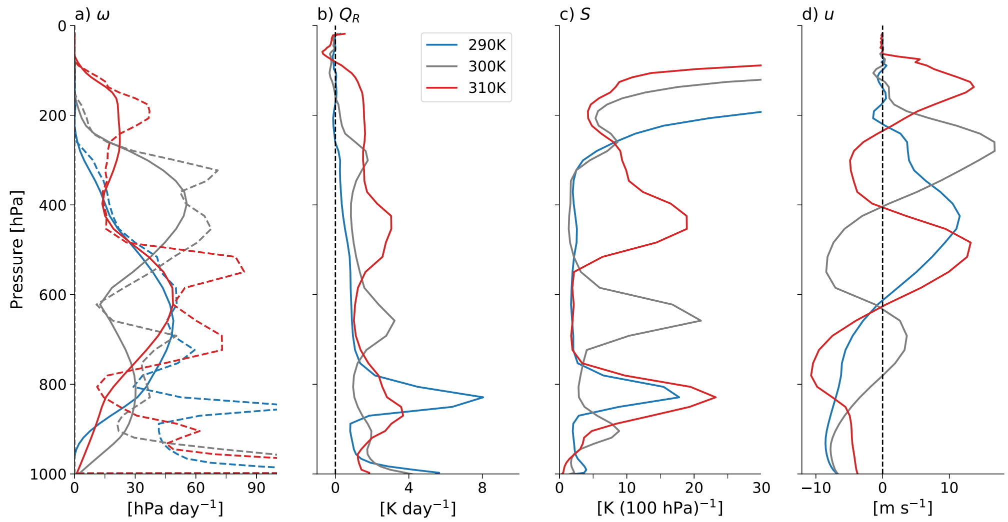

Figure 8. a) Pressure velocity ω in the cold pool regions of the 290K 3D simulation (blue), the control simulation (gray) and the 310K simulation (red). The dashed lines show implied velocities based on WTG balance and the cold pool region is defined as $x = 10{\times}10^3$km to $12{\times}10^3$km. b) Radiative heating profiles for the same simulations. c) Stability S in the same simulations. d) Horizontal velocities in the same simulations, averaged over $x = 6{\times}10^3$km to $8{\times}10^3$km.

be slightly higher than the radiative cooling maximum, a subtlety which must be captured to explain the double cell.

So, while double cells are clearly favored at warmer SSTs and by the presence of extreme dryness over the cold pool, more work is needed to fully understand why the circulation transitions to a double cell, why the transition occurs near mean SSTs of 300K and why the tropical Pacific is less favorable for the development of double-cells. Idealized calculations with a radiative transfer model show that greater humidity levels make the maximum in Q_R less pronounced (not shown), though this would also affect the stability. We note that present-day temperatures over the equatorial Pacific are close to the transition from single to double cell circulations, and we cannot rule out the possibility of the observed Walker circulation transitioning to a double cell for large enough tropical warming.

5.1 Fixed radiative cooling simulations

Several past studies of mock-Walker simulations have eliminated double cells by prescribing vertically-uniform radiative cooling profiles [e.g., *Grabowski et al.*, 2000; *Wofsy and*

Kuang, 2012; *Slawinska et al.*, 2014]. This modifies the radiative-subsidence balance to:

$$\omega_R(p) = Q_{R0}/S(p), \tag{2}$$

so that the vertical structure of ω_R is determined by the inverse of the stability. But even with prescribed radiation, it is possible to generate double-cell circulations at warm enough SSTs, because the stability S develops a mid-tropospheric maximum, and this maximum strengthens and rises as the surface temperature is increased (see Appendix A).

To demonstrate this, we have run 2D mock-Walker simulations with fixed radiative cooling profiles, varying the mean SST from 300K to 310K (apart from the fixed radiative cooling, the model set-up is identical to the 2D mock-Walker simulations in *Lutsko and Cronin* [2018]). At 300K the circulation has a single overturning cell, which transitions to a double overturning cell at 310K (Figure 9). The 305K simulation is an intermediate case, and resembles the control 3D mock-Walker simulation in Figure 4. Hence fixed radiative cooling simulations are less likely to exhibit a double overturning cell than simulations with interactive radiation at present-day SSTs, but a double cell does still appear at warm enough SSTs.

6 Conclusion

In this study, we have investigated the mean climate and dynamics of mock-Walker simulations, as well as their responses to warming, motivated by the need for modelling set-ups that explicitly simulate both convective systems and large-scale atmospheric flows. By prescribing a horizontally-varying SST profile, the flow in mock-Walker simulations is constrained to resemble that over the tropical Pacific, with ascent over the warm pool and subsidence over the cold pool.

Mock-Walker simulations with realistic SST profiles qualitatively reproduce many observed features of the atmosphere over the tropical Pacific, such as zonal profiles of precipitation and net cloud radiative effect. However, the flows in these simulation tend to consist of two vertically-stacked cells in much of the domain, rather than the single cells seen in reanalysis. Simulations across a range of SSTs indicate that these simulations are part of a larger transition from a single overturning cell at colder SSTs to a double overturning cell at warmer SSTs, with the transition occurring near the present-day mean eastern Pacific SST of ~300K. The upper tropospheres over the cold pools of the mock-Walker simulations also show extreme dryness (relative humidities of less than 10%) compared to reanalysis, as well

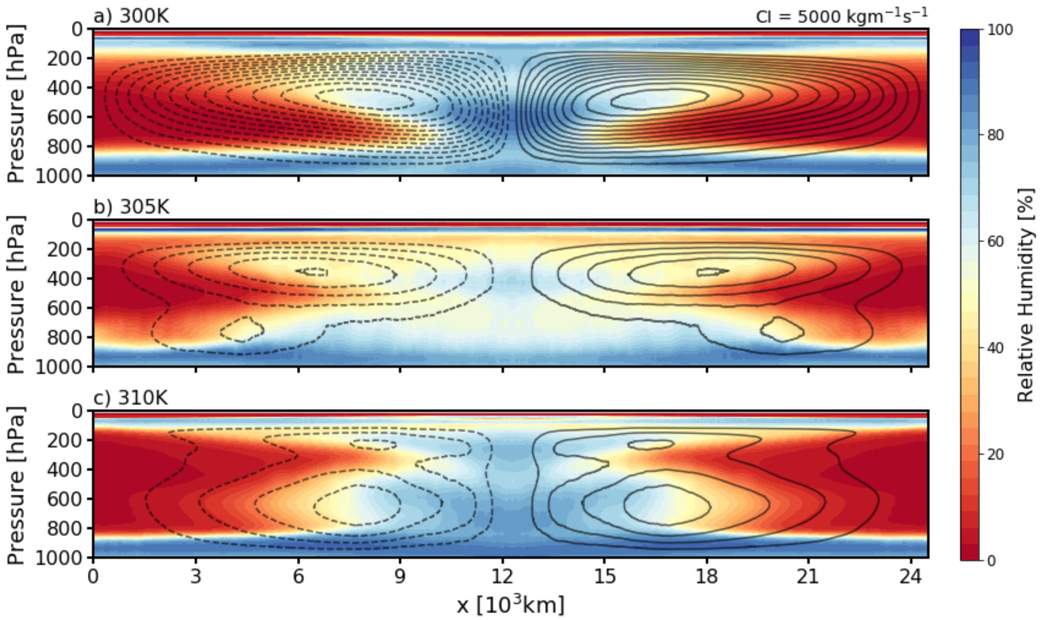

Figure 9. a) Mean relative humidity (colored contours) and streamfunction (black contours) for the 2D SAM simulation with a mean SST of 300K and a fixed radiative cooling of 1.5K/day in the troposphere, linearly decreasing to 0K/day between 185hPa and 140hPa. b) Same as panel a) but for a simulation with a mean SST of 305K. c) Same as panel a) but for a simulation with a mean SST of 310K. The same contour interval is used in all panels

as weaker LW CRE and a more negative net CRE compared to satellite observations. We have been unable to find in-situ observations from the Eastern Pacific to further validate the realism of the mock-Walker simulations relative to reanalysis, and note that reanalysis might not represent nuances of humidity or vertical velocities well in this region due to the lack of observational constraints.

The response of mock-Walker simulations to uniform warming is largely governed by circulation changes. For moderate and strong SST gradients (our control and La Niña cases), the lower circulation cell strengthens and expands upwards, with consequences for the vertical structure of domain-averaged temperature and relative humidity. By contrast, for a weaker SST gradient (our El Niño case), the circulation changes are weak, and the temperature response resembles warming of a moist adiabat. The largest tropospheric warming is seen for the La Niña case, which also features the most organized convection. The SST gradient also has a strong effect on the net climate feedback, which varies considerably across the simulations, from -0.49Wm^{-2}K^{-1} for the El Niño case to -3.49Wm^{-2}K^{-1} in the La Niña case, corresponding to a seven-fold change in climate sensitivity. The spread in the net climate feedback is driven primarily by differences in the net cloud feedback, which arise from circulation changes. Patterned warming can either strengthen the feedback – if the zonal SST gradient is increased – or weaken the feedback – if the zonal SST gradient is weakened. However, we caution again that these simulations are highly idealized and the sensitivities should not be taken literally, though they are consistent with previous work suggesting that stronger SST gradients are associated with weaker climate sensitivities.

The transition to a double-cell circulation at warm SSTs can be understood using Weak Temperature Gradient balance, as the implied radiative-subsidence velocities qualitatively reproduce the full vertical velocities in the cold pool regions. However, the vertical profiles of radiative cooling and stability are complex, and we have been unable to capture their behavior with a simple model. The double cells do seem to be associated with the extreme dryness of the upper troposphere over the cold pools of the simulations, and the fact that double cells are less favored in the observed tropical Pacific is likely related to the cold pool being moister than in our simulations. For example, the cold pool in the east Pacific was very dry in October 1995, and the flow showed hints of a double cell (Figure 4c). In June 1996 the cold pool was less dry and the flow was single-celled (Figure 4a).

Finally, previous studies have eliminated double cells by prescribing radiative cooling profiles, but we have shown that a double cell does still develop for sufficiently warm underlying SSTs. With vertically-uniform cooling, the transition to a double cell occurs near 305K in 2D mock-Walker simulations (rather than 300K with interactive radiation) and is caused by the development of a stability maximum, which strengthens and rises for warmer SSTs.

These results highlight some of the strengths and limitations of mock-Walker simulations. On the one hand, they can qualitatively reproduce the observed tropical Pacific climate, and they force the convection to organize over the warmest SSTs, eliminating the ambiguity around how to interpret convective organization in uniform SST simulations. On the other hand, the results presented here suggest that the double-cell circulation, and their increasing prominence with warming, may limit the utility of mock-Walker simulations for studying realistic cloud feedbacks and for studying the interactions between clouds and tropical circulations. Further study of the circulation in the mock-Walker setup is needed in order

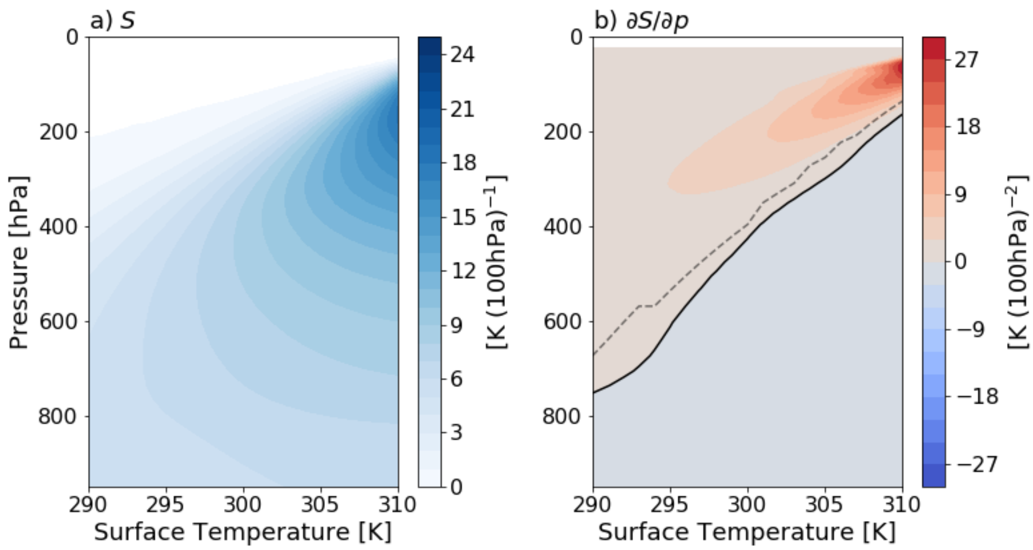

Figure A.1. a) Stability S of a moist pseudoadiabatic column as a function of surface temperature. The stratosphere is assumed to be isothermal, with temperature 200K. b) $\partial S/\partial p$ for the same columns. The thick black line shows where $\partial S/\partial p = 0$ and the thin dashed black line shows the values predicted by equation A.3.

to help understand how the Earth's real Walker circulation might change with climate – either to rule out the strong circulation changes we have found, or to determine that they are in fact physically plausible.

A: Development of a stability maximum at warm SSTs

The stability S of an atmospheric column can be written as:

$$S = -\frac{1}{c_p}\frac{\partial D}{\partial p} = \left(\Gamma_{z,d} - \Gamma_z\right)\frac{\partial z}{\partial p} = \Delta\Gamma_z \frac{\partial z}{\partial p}, \tag{A.1}$$

where $D = c_p T + gz$ is the dry static energy, $\Gamma_z = \partial T/\partial z$ and $\Gamma_{z,d} = -g/c_p$. In this formulation, the stability is the difference between the dry adiabatic temperature lapse-rate and the temperature lapse-rate, divided by the rate of change of the atmosphere's mass with height. As surface temperature is warmed, the rate at which the lapse-rate converges to the dry adiabatic decreases, causing $\partial S/\partial p$ to change sign and a stability maximum to develop. Figure A.1 shows that for a moist, pseudoadiabatic column there is a maximum at 850hPa for a surface temperature of 290K, which strengthens and migrates upwards as the surface is warmed.

To better understand the development of stability maxima, we approximate atmospheric pressure as $p \approx p_0 e^{-z/H}$, where $H = R_d T/g$ is the pressure scale height, R_d is the dry gas constant and p_0 is a reference pressure. Substituting into A.1 gives:

$$S \approx \frac{H\Delta\Gamma_z}{p}, \tag{A.2}$$

and so:

$$\frac{\partial S}{\partial p} \approx \frac{H}{p}\left(\frac{\partial \Delta\Gamma_z}{\partial p} - \frac{\Delta\Gamma_z}{p}\right). \tag{A.3}$$

The dashed line in Figure A1b shows this approximation accurately captures the rising position of the stability maximum as surface temperature is increased, such that the stability maximum develops when the lapse rate converges to the dry adiabat at a rate of $\Delta\Gamma_z/p$.

Acknowledgments

This work was supported by NSF grant AGS-1623218, "Collaborative Research: Using a Hierarchy of Models to Constrain the Temperature Dependence of Climate Sensitivity". The System for Atmospheric Modeling code is available from http://rossby.msrc.sunysb.edu/~marat/SAM.html. Namelist files for all of the simulations presented and analysis scripts will be made publicly available on acceptance of the manuscript.

References

Abbott, T. H., T. W. Cronin, and T. Beucler (2020), Convective Dynamics and the Response of Precipitation Extremes to Warming in Radiative–Convective Equilibrium, *Journal of the Atmospheric Sciences*, *77*(5), 1637–1660, doi:10.1175/JAS-D-19-0197.1.

Andrews, T., and M. J. Webb (2018), The dependence of global cloud and lapse rate feedbacks on the spatial structure of tropical pacific warming, *Journal of Climate*, *31*(7), 641–654.

Andrews, T., J. M. Gregory, and M. J. Webb (2015), The dependence of radiative forcing and feedback on evolving patterns of surface temperature change in climate models., *Journal of Climate*, *28*(2), 1630–1648.

Andrews, T., J. M. Gregory, D. Paynter, L. G. Silvers, C. Zhou, T. Mauritsen, M. J. Webb, K. C. Armour, P. M. Forster, and H. Titchner (2018), Accounting for Changing Temperature Patterns Increases Historical Estimates of Climate Sensitivity, *Geophysical Research Letters*, *45*(16), 8490–8499.

Andrews, T., A. Bodas-Salcedo, J. M. Gregory, Y. Dong, K. C. Armour, D. Paynter, P. Lin, A. Modak, T. Mauritsen, J. N. S. Cole, B. Medeiros, J. J. Benedict, H. Douville, R. Roehrig, T. Koshiro, H. Kawai, T. Ogura, J.-L. Dufresne, R. P. Allan, and C. Liu (2022), On the Effect of Historical SST Patterns on Radiative Feedback, *Journal of Geophysical Research: Atmospheres*, *127*(18), e2022JD036,675, doi:10.1029/2022JD036675, _eprint: https://onlinelibrary.wiley.com/doi/pdf/10.1029/2022JD036675.

Armour, K. C., C. M. Bitz, and G. H. Roe (2013), Time-Varying Climate Sensitivity from Regional Feedbacks, *Journal of Climate*, *26*, 4518–4534.

Arnold, N. P., and D. A. Randall (2015), Global-scale convective aggregation: Implications for the madden-julian oscillation, *Journal of Advances in Modeling Earth Systems*, *7*(4), 1499–1518.

Back, L. E., and C. S. Bretherton (2006), Geographic variability in the export of moist static energy and vertical motion profiles in the tropical Pacific, *Geophysical Research Letters*, *33*(17), L17,810.

Beucler, T., T. H. Abbott, T. W. Cronin, and M. S. Pritchard (2019), Comparing convective self?aggregation in idealized models to observed moist static energy variability near the equator, *Geophysical Research Letters*, *46*, 10,589–10,598.

Bloch-Johnson, J., M. Rugenstein, and D. S. Abbot (2020), Spatial Radiative Feedbacks from Internal Variability Using Multiple Regression, *Journal of Climate*, *33*(10), 4121–4140, doi:10.1175/JCLI-D-19-0396.1.

Bony, S., B. Stevens, D. M. W. Frierson, C. Jakob, M. Kageyama, R. Pincus, T. G. Shepherd, S. C. Sherwood, A. P. Siebesma, A. H. Sobel, M. Watanabe, and M. J. Webb (2015), Clouds, circulation and climate sensitivity, *Nature Geoscience*, *8*(4), 261–268, doi: 10.1038/ngeo2398.

Bretherton, C. S., and A. H. Sobel (2002), A Simple Model of a Convectively Coupled Walker Circulation Using the Weak Temperature Gradient Approximation, *Journal of Climate*, *15*, 14.

Bretherton, C. S., P. N. Blossey, and M. E. Peters (2006), Interpretation of simple and cloud-resolving simulations of moist convection-radiation interaction with a mock-Walker circulation, *Theoretical and Computational Fluid Dynamics*, *20*(5-6), 421–442, doi: 10.1007/s00162-006-0029-7.

Ceppi, P., and S. Fueglistaler (2021), The El Niño–Southern Oscillation Pattern Effect, *Geophysical Research Letters*, *48*(21), e2021GL095,261, doi:10.1029/2021GL095261, _eprint: https://onlinelibrary.wiley.com/doi/pdf/10.1029/2021GL095261.

Ceppi, P., and J. M. Gregory (2017), Relationship of tropospheric stability to climate sensitivity and Earth's observed radiation budget, *Proceedings of the National Academy of Sciences*, *114*(50), 13,126–13,131.

Cess, R. D., and G. L. Potter (1988), A methodology for understanding and intercomparing atmospheric climate feedback processes in general circulation models., *Journal of Geophysical Research*, *93*, 8305–8314.

Collins, W. D., P. J. Rasch, B. A. Boville, J. J. Hack, J. R. McCaa, D. L. Williamson, B. P. Briegleg, C. M. Bitz, S. J. Lin, and M. Zhang (2006), The formulation and atmospheric simulation of the community atmosphere model version 3 (cam3)., *Journal of Climate*, *19*, 2144–2161.

Coppin, D., and S. Bony (2015), Physical mechanisms controlling the initiation of convective self-aggregation in a general circulation model, *Journal of Advances in Modeling Earth Systems*, *7*(4), 2060–2078.

Cronin, T. W. (2014), On the Choice of Average Solar Zenith Angle, *Journal of the Atmospheric Sciences*, *71*(8), 2994–3003.

Cronin, T. W., and A. A. Wing (2017), Clouds, circulation, and climate sensitivity in a radiative-convective equilibrium channel model., *Journal of Advances in Modeling Earth Systems*, *9*(5), 2883–2905.

Dong, Y., C. Proistosescu, K. C. Armour, and D. S. Battisti (2019), Attributing Historical and Future Evolution of Radiative Feedbacks to Regional Warming Patterns using a Green's Function Approach: The Preeminence of the Western Pacific, *Journal of Climate*, *32*(17), 5471–5491.

Dong, Y., K. C. Armour, M. D. Zelinka, C. Proistosescu, D. S. Battisti, C. Zhou, and T. Andrews (2020), Intermodel Spread in the Pattern Effect and Its Contribution to Climate Sensitivity in CMIP5 and CMIP6 Models, *Journal of Climate*, *33*(18), 7755–7775, doi: 10.1175/JCLI-D-19-1011.1, publisher: American Meteorological Society Section: Journal of Climate.

Dong, Y., K. C. Armour, C. Proistosescu, T. Andrews, D. S. Battisti, P. M. Forster, D. Paynter, C. J. Smith, and H. Shiogama (2021), Biased Estimates of Equilibrium Climate Sensitivity and Transient Climate Response Derived From Historical CMIP6 Simulations, *Geophysical Research Letters*, *48*(24), e2021GL095,778, doi:10.1029/2021GL095778, _eprint: https://onlinelibrary.wiley.com/doi/pdf/10.1029/2021GL095778.

Emanuel, K. (2019), Inferences from Simple Models of Slow, Convectively Coupled Processes, *Journal of the Atmospheric Sciences*, *76*(1), 195–208.

Forster, P. M., T. Andrews, P. Good, J. M. Gregory, L. S. Jackson, and M. Zelinka (2013), Evaluating adjusted forcing and model spread for historical and future scenarios in the cmip5 generation of climate models, *Journal of Geophysical Research: Atmospheres*, *118*, 1139–1150.

Grabowski, W., and M. Moncrieff (2001), Large-scale organization of tropical convection in two-dimensional explicit numerical simulations, *Q. J. R. Meteorol. Soc.*, *127*, 445–468.

Grabowski, W., and M. Moncrieff (2002), Large-scale organization of tropical convection in two-dimensional explicit numerical simulations: Effects of interactive radiation, *Q. J. R. Meteorol. Soc.*, *128*, 2349–2375.

Grabowski, W. W., J.-I. Yano, and M. W. Moncrieff (2000), Cloud resolving modeling of tropical circulations driven by large-scale sst gradients, *Journal of the Atmospheric Sciences*, *57*(23), 2022–2039.

Harrop, B. E., and D. L. Hartmann (2016), The role of cloud radiative heating within the atmosphere on the high cloud amount and top-of-atmosphere cloud radiative effect, *Journal of Advances in Modeling Earth Systems*, *8*(23), 1391–1410.

Hartmann, D. L., and B. D. Dygert (2022), Global Radiative Convective Equilibrium With a Slab Ocean: SST Contrast, Sensitivity and Circulation, *Journal of Geophysical Research: Atmospheres*, *127*(12), e2021JD036,400, doi:10.1029/2021JD036400, _eprint: https://onlinelibrary.wiley.com/doi/pdf/10.1029/2021JD036400.

Hartmann, D. L., and K. Larson (2002), An important constraint on tropical cloud - climate feedback: TROPICAL CLOUD-CLIMATE FEEDBACK, *Geophysical Research Letters*, *29*(20), 1–4, doi:10.1029/2002GL015835.

Hartmann, D. L., P. N. Blossey, and B. D. Dygert (2019), Convection and Climate: What Have We Learned from Simple Models and Simplified Settings?, *Current Climate Change Reports*, *5*(3), doi:10.1007/s40641-019-00136-9.

Hersbach, H., B. Bell, P. Berrisford, S. Hirahara, A. Horányi, J. Muñoz-Sabater, J. Nicolas, C. Peubey, R. Radu, D. Schepers, A. Simmons, C. Soci, S. Abdalla, X. Abellan, G. Balsamo, P. Bechtold, G. Biavati, J. Bidlot, M. Bonavita, G. De Chiara, P. Dahlgren, D. Dee, M. Diamantakis, R. Dragani, J. Flemming, R. Forbes, M. Fuentes, A. Geer, L. Haimberger, S. Healy, R. J. Hogan, E. Hólm, M. Janisková, S. Keeley, P. Laloyaux, P. Lopez, C. Lupu, G. Radnoti, P. de Rosnay, I. Rozum, F. Vamborg, S. Villaume, and J.-N. Thépaut

(2020), The era5 global reanalysis, *Quarterly Journal of the Royal Meteorological Society*, *146*(730), 1999–2049, doi:https://doi.org/10.1002/qj.3803.

Holloway, C. E., A. A. Wing, S. Bony, C. Muller, H. Masunaga, T. S. L'Ecuyer, D. D. Turner, and P. Zuidema (2017), Observing convective aggregation, *Surveys of Geophysics*, *38*, 1199–1236.

Iipponen, J., and L. Donner (2020), Simple Analytic Solutions for a Convectively Driven Walker Circulation and Their Relevance to Observations, *Journal of the Atmospheric Sciences*, *78*(1), 299–311, doi:10.1175/JAS-D-20-0014.1.

Inoue, K., and L. E. Back (2015), Gross Moist Stability Assessment during TOGA COARE: Various Interpretations of Gross Moist Stability, *Journal of the Atmospheric Sciences*, *72*(11), 4148–4166.

Jeevanjee, N., and S. Fueglistaler (2020), Simple Spectral Models for Atmospheric Radiative Cooling, *Journal of the Atmospheric Sciences*, *77*(2), 479–497, doi:10.1175/JAS-D-18-0347.1.

Khairoutdinov, M. F., and D. A. Randall (2003), Cloud resolving modeling of the arm summer 1997 iop: Model formulation, results, uncertainties, and sensitivities, *Journal of the Atmospheric Sciences*, *60*(23), 607–625.

Kuang, Z. (2012), Weakly Forced Mock Walker Cells, *Journal of the Atmospheric Sciences*, *69*(9), 2759–2786.

Larson, K., and D. L. Hartmann (2003), Interactions among cloud, water vapor, radiation, and large-scale circulation in the tropical climate. part ii: Sensitivity to spatial gradients of sea surface temperature., *Journal of Climate*, *16*(10), 1441–1455.

Lindzen, R. S., and S. Nigam (1987), On the role of sea surface temperature gradients in forcing low level winds and convergence in the tropics, *Journal of the Atmospheric Sciences*, *44*(23), 2418–2436.

Liu, C., and M. W. Moncrieff (2008), Explicitly simulated tropical convection over idealized warm pools, *Journal of Geophysical Research: Atmospheres*, *113*(D21).

Lloyd, J., E. Guilyardi, and H. Weller (2012), The Role of Atmosphere Feedbacks during ENSO in the CMIP3 Models. Part III: The Shortwave Flux Feedback, *Journal of Climate*, *25*(12), 4275–4293.

Lutsko, N. J. (2018), The Relationship Between Cloud Radiative Effect and Surface Temperature Variability at El Niño-Southern Oscillation Frequencies in CMIP5 Models, *Geophysical Research Letters*, *45*(19), 10,599–10,608, doi:10.1029/2018GL079236.

Lutsko, N. J., and T. W. Cronin (2018), Increase in Precipitation Efficiency With Surface Warming in Radiative-Convective Equilibrium, *Journal of Advances in Modeling Earth Systems*, *10*(11), 2992–3010, doi:10.1029/2018MS001482.

Mapes, B. (2001), Water's two height scales: The moist adiabat and the radiative troposphere, *Quarterly Journal of the Royal Meteorological Society*, *127*(141), 2353–2366.

Meraner, K., T. Mauritsen, and A. Voigt (2013), Robust increase in equilibrium climate sensitivity under global warming, *Geophysical Research Letters*, *40*(22), 5944–5948.

Merlis, T. M., and T. Schneider (2011), Changes in zonal surface temperature gradients and walker circulations in a wide range of climates, *Journal of Climate*, *24*(17), 4757–4768.

Middlemas, E. A., A. C. Clement, B. Medeiros, and B. Kirtman (2019), Cloud Radiative Feedbacks and El Niño–Southern Oscillation, *Journal of Climate*, *32*(15), 4661–4680, doi: 10.1175/JCLI-D-18-0842.1, publisher: American Meteorological Society Section: Journal of Climate.

Muller, C. J., and I. M. Held (2012), Detailed Investigation of the Self-Aggregation of Convection in Cloud-Resolving Simulations, *Journal of the Atmospheric Sciences*, *69*(8), 2551–2565, doi:10.1175/JAS-D-11-0257.1.

Muller, C. J., P. A. O'Gorman, and L. E. Back (2011), Intensification of Precipitation Extremes with Warming in a Cloud-Resolving Model, *Journal of Climate*, *24*(11), 2784–2800, doi:10.1175/2011JCLI3876.1.

Murphy, D. M., and T. Koop (2005), Review of the vapour pressures of ice and supercooled water for atmospheric applications, *Quarterly Journal of the Royal Meteorological Society*, *131*(608), 1539–1565.

Park, S., and C. B. Leovy (2004), Marine Low-Cloud Anomalies Associated with ENSO, *JOURNAL OF CLIMATE*, *17*, 22.

Pendergrass, A. G., K. A. Reed, and B. Medeiros (2016), The link between extreme precipitation and convective organization in a warming climate: Global radiative-convective equilibrium simulations, *Geophysical Research Letters*, *43*(21), 11,445–11,452.

Peters, M. E., and C. S. Bretherton (2005), A Simplified Model of the Walker Circulation with an Interactive Ocean Mixed Layer and Cloud-Radiative Feedbacks, *Journal of Climate*, *18*(20), 4216–4234.

Popp, M., and S. Bony (2019), Stronger zonal convective clustering associated with a wider tropical rain belt, *Nature Communications*, *10*(1), 4261, doi:10.1038/s41467-019-12167-9.

Popp, M., N. J. Lutsko, and S. Bony (2020), The Relationship Between Convective Clustering and Mean Tropical Climate in Aquaplanet Simulations, *Journal of Advances in Modeling Earth Systems*, *12*(8), e2020MS002,070, doi:https://doi.org/10.1029/2020MS002070, _eprint: https://agupubs.onlinelibrary.wiley.com/doi/pdf/10.1029/2020MS002070.

Posselt, D. J., S. C. v. d. Heever, and G. L. Stephens (2008), Trimodal cloudiness and tropical stable layers in simulations of radiative convective equilibrium, *Geophysical Research Letters*, *35*(8).

Posselt, D. J., S. v. d. Heever, G. Stephens, and M. R. Igel (2012), Changes in the Interaction between Tropical Convection, Radiation, and the Large-Scale Circulation in a Warming Environment, *Journal of Climate*, *25*(2), 557–571.

Radley, C., S. Fueglistaler, and L. Donner (2014), Cloud and Radiative Balance Changes in Response to ENSO in Observations and Models, *Journal of Climate*, *27*(9), 3100–3113, doi:10.1175/JCLI-D-13-00338.1, publisher: American Meteorological Society Section: Journal of Climate.

Randall, D., M. Khairoutdinov, A. Arakawa, and W. Grabowski (2003), Breaking the Cloud Parameterization Deadlock, *Bulletin of the American Meteorological Society*, *84*(11), 1547–1564, doi:10.1175/BAMS-84-11-1547.

Reed, K. A., B. Medeiros, J. T. Bacmeister, and P. H. Lauritzen (2015), Global radiative–convective equilibrium in the community atmosphere model, version 5, *Journal of the Atmospheric Sciences*, *72*(15), 2183–2187.

Romps, D. M. (2014), An analytical model for tropical relative humidity., *Journal of Climate*, *27*(23), 7432–7449.

Ruppert Jr, J. H., and C. Hohenegger (2018), Diurnal circulation adjustment and organized deep convection, *Journal of Climate*, *31*(23), 4899–4916.

Schneider, T., J. Teixeira, C. S. Bretherton, F. Brient, K. G. Pressel, C. Schär, and A. P. Siebesma (2017), Climate goals and computing the future of clouds, *Nature Climate Change*, *7*(1), 3–5, doi:10.1038/nclimate3190.

Seeley, J. T., and D. M. Romps (2015), Why does tropical convective available potential energy (CAPE) increase with warming?, *Geophysical Research Letters*, *42*(23), 10,429–10,437, doi:10.1002/2015GL066199.

Seeley, J. T., N. Jeevanjee, and D. M. Romps (2019), FAT or FiTT: Are Anvil Clouds or the Tropopause Temperature Invariant?, *Geophysical Research Letters*, *46*(3), 1842–1850, doi:10.1029/2018GL080096.

Sherwood, S. C., M. J. Webb, J. D. Annan, K. C. Armour, P. M. Forster, J. C. Hargreaves, G. Hegerl, S. A. Klein, K. D. Marvel, E. J. Rohling, M. Watanabe, T. Andrews, P. Braconnot, C. S. Bretherton, G. L. Foster, Z. Hausfather, A. S. v. d. Heydt, R. Knutti, T. Mauritsen, J. R. Norris, C. Proistosescu, M. Rugenstein, G. A. Schmidt, K. B. Tokarska, and M. D. Zelinka (2020), An assessment of Earth's climate sensitivity using multiple lines of evidence, *Reviews of Geophysics*, *n/a*(n/a), e2019RG000,678.

Silvers, L. G., and T. Robinson (2021), Clouds and Radiation in a mock-Walker Circulation, *Journal of Advances in Modeling Earth Systems*, *n/a*(n/a), e2020MS002,196, doi: https://doi.org/10.1029/2020MS002196.

Silvers, L. G., D. Paynter, and M. Zhao (2018), The diversity of cloud responses to twentieth century sea surface temperatures, *Geophysical Research Letters*, *45*(1), 391–400, 2017GL075583.

Singh, M. S., and P. A. O'Gorman (2013), Influence of entrainment on the thermal stratification in simulations of radiative-convective equilibrium, *Geophysical Research Letters*, *40*(16), 4398–4403, doi:10.1002/grl.50796.

Slawinska, J., O. Pauluis, A. J. Majda, and W. W. Graboskwi (2014), Multiscale interactions in an idealized walker circulation: Mean circulation and intraseasonal variability, *Journal of the Atmospheric Sciences*, *71*(3), 953–971.

Soden, B. J., and I. M. Held (2006), An assessment of climate feedbacks in coupled ocean-atmosphere models, *Journal of Climate*, *19*(6), 3354–3360.

Stephens, G. L., S. van den Heever, and L. Pakula (2008), Radiative–Convective Feedbacks in Idealized States of Radiative–Convective Equilibrium, *Journal of the Atmospheric Sciences*, *65*(12), 3899–3916.

Stevens, B., and S. Bony (2013), What Are Climate Models Missing?, *Science*, *340*(6136), 1053–1054, doi:10.1126/science.1237554.

Stevens, B., S. C. Sherwood, S. Bony, and M. J. Webb (2016), Prospects for narrowing bounds on Earth's equilibrium climate sensitivity, *Earth's Future*, *4*(11), 512–522, doi:10.1002/2016EF000376, _eprint: https://onlinelibrary.wiley.com/doi/pdf/10.1002/2016EF000376.

Tompkins, A. M., and G. C. Craig (1998), Radiative-convective equilibrium in a three-dimensional cloud-ensemble model, *Quarterly Journal of the Royal Meteorological Society*, *124*(23), 2073–2097.

Vial, J., J.-L. Dufreshne, and S. Bony (2013), On the interpretation of inter-model spread in cmip5 climate sensitivity estimates., *Climate Dynamics*, *41*(1), 3339–3362.

Wing, A. A. (2019), Self-aggregation of deep convection and its implications for climate, *Current Climate Change Reports*, *5*(2), 1–11.

Wing, A. A., and T. W. Cronin (2016), Self aggregation in long channel geometry., *Quarterly Journal of the Royal Meteorological Society*, *142*(5), 1–15.

Wing, A. A., and K. A. Emanuel (2014), Physical mechanisms controlling self-aggregation of convection in idealized numerical modeling simulations, *Journal of Advances in Modeling Earth Systems*, *6*(1), 59–74, doi:10.1002/2013MS000269.

Wing, A. A., K. A. Reed, M. Satoh, B. Stevens, S. Bony, and T. Ohno (2018a), Radiative-convective equilibrium model intercomparison project, *Geoscientific Model Development*, *11*(2), 793–813.

Wing, A. A., K. A. Reed, M. Satoh, B. Stevens, S. Bony, and T. Ohno (2018b), Radiative–convective equilibrium model intercomparison project, *Geoscientific Model Development*, *11*(2), 793–813, doi:10.5194/gmd-11-793-2018.

Wing, A. A., C. L. Stauffer, T. Becker, K. A. Reed, M.-S. Ahn, N. P. Arnold, S. Bony, M. Branson, G. H. Bryan, J.-P. Chaboureau, S. R. De Roode, K. Gayatri, C. Hohenegger, I.-K. Hu, F. Jansson, T. R. Jones, M. Khairoutdinov, D. Kim, Z. K. Martin, S. Matsugishi, B. Medeiros, H. Miura, Y. Moon, S. K. Müller, T. Ohno, M. Popp, T. Prabhakaran, D. Randall, R. Rios-Berrios, N. Rochetin, R. Roehrig, D. M. Romps, J. H. Ruppert Jr., M. Satoh, L. G. Silvers, M. S. Singh, B. Stevens, L. Tomassini, C. C. van Heerwaarden, S. Wang, and M. Zhao (2020), Clouds and Convective Self-Aggregation in a Multimodel Ensemble of Radiative-Convective Equilibrium Simulations, *Journal of Advances in Modeling Earth Systems*, *12*(9), e2020MS002,138, doi:10.1029/2020MS002138, _eprint: https://onlinelibrary.wiley.com/doi/pdf/10.1029/2020MS002138.

Wofsy, J., and Z. Kuang (2012), Cloud-resolving model simulations and a simple model of an idealized walker cell, *Journal of Climate*, *25*(10), 8090–8106.

Yano, J.-I., W. W. Grabowski, and M. W. Moncrieff (2002a), Mean-state convective circulations over large-scale tropical sst gradients, *Journal of the Atmospheric Sciences*, *59*(23), 1578–1592.

Yano, J.-I., M. W. Moncrieff, and W. W. Grabowski (2002b), Walker-Type Mean Circulations and Convectively Coupled Tropical Waves as an Interacting System, *Journal of the Atmospheric Sciences*, *59*, 1566–1577.

Zhang, C., and M. McGauley (2004), Shallow Meridional Circulation in the Tropical Eastern Pacific, *Journal of Climate*, *17*, 7.

Zhou, C., M. D. Zelinka, and S. A. Klein (2017), Analyzing the dependence of global cloud feedback on the spatial pattern of sea surface temperature change with a green's function approach, *Journal of Advances in Modeling Earth Systems*, *9*(23), 2174–2189.

Figure 1.

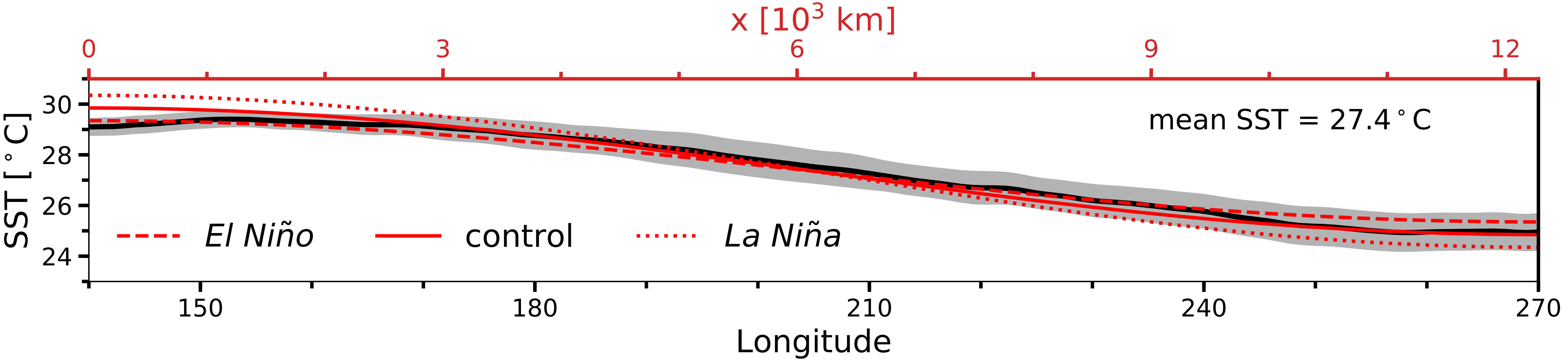

x [10^3 km]
0
3
6
9
12
30
28
26
24
SST [$^\circ$C]
mean SST = 27.4°C
El Niño
control
La Niña
150
180
210
240
270
Longitude

Figure 2.

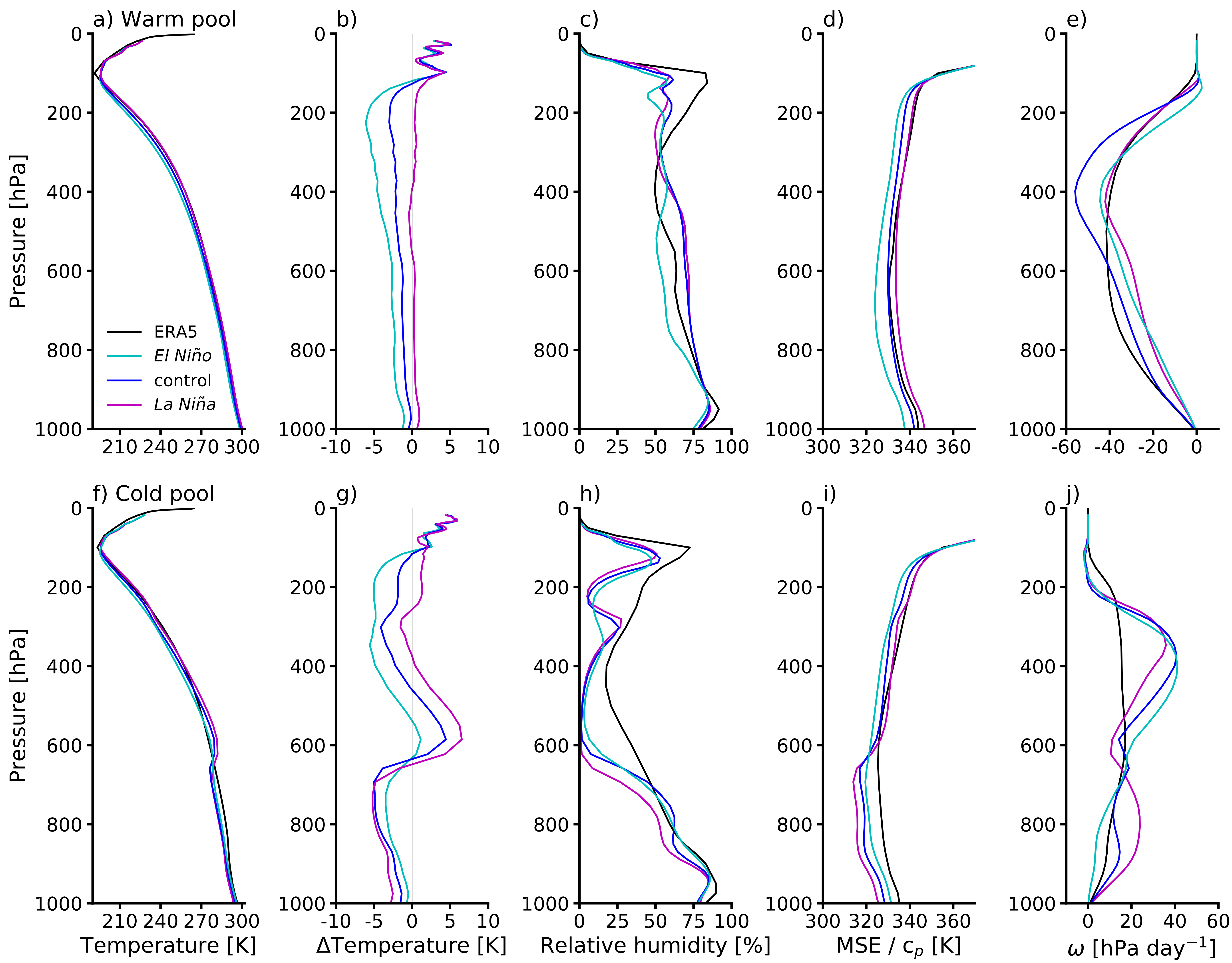

a) Warm pool
b)
c)
d)
e)
f) Cold pool
g)
h)
i)
j)
ERA5
El Niño
control
La Niña
Pressure [hPa]
Temperature [K]
ΔTemperature [K]
Relative humidity [%]
MSE / c_p [K]
ω [hPa day^-1]

Figure 3.

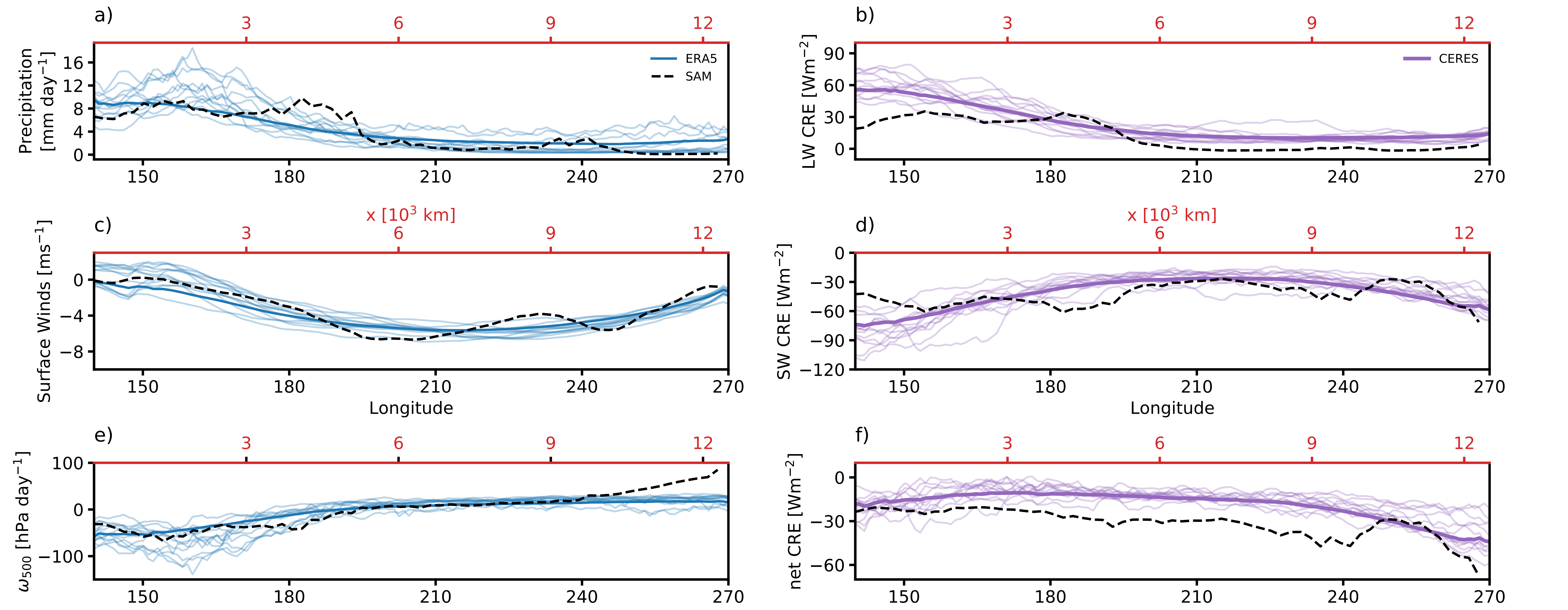

a)
b)
c)
d)
e)
f)
ERA5
SAM
CERES
Precipitation [mm day^{-1}]
LW CRE [Wm^{-2}]
Surface Winds [ms^{-1}]
SW CRE [Wm^{-2}]
ω_{500} [hPa day^{-1}]
net CRE [Wm^{-2}]
x [10^3 km]
Longitude

Figure 4.

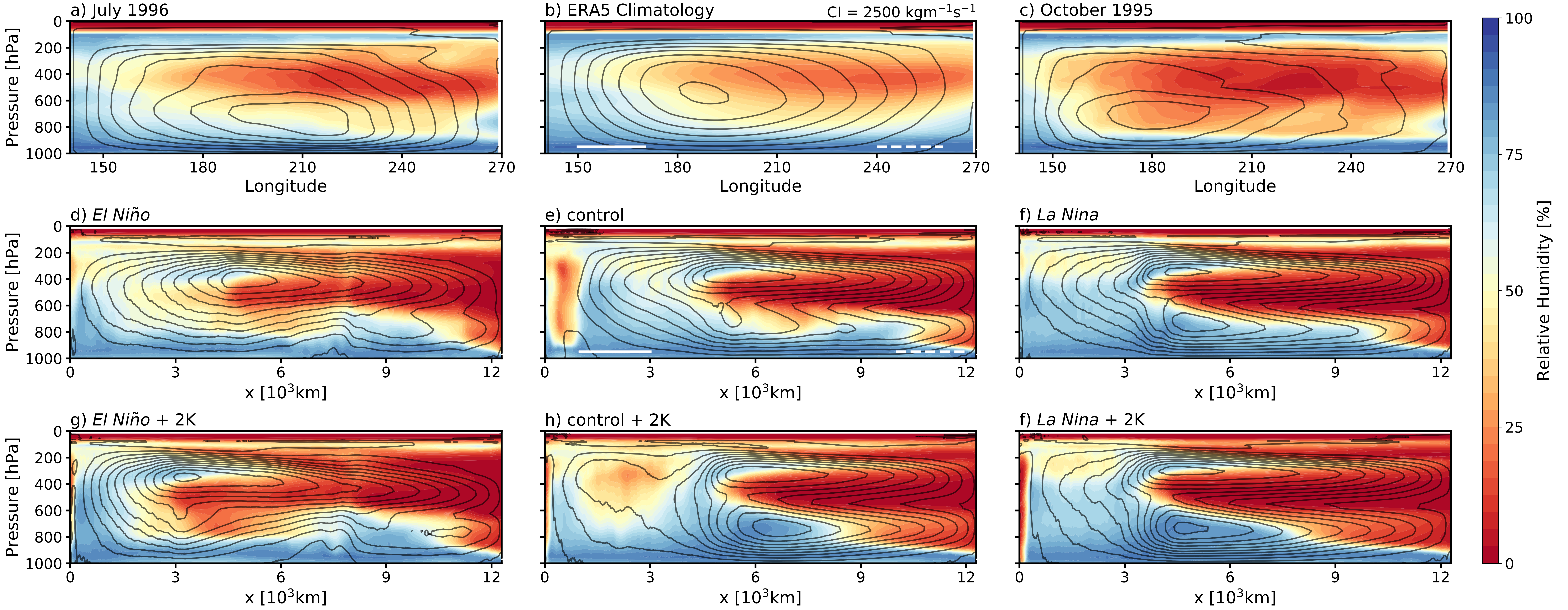
a) July 1996
b) ERA5 Climatology
CI = 2500 kgm⁻¹s⁻¹
c) October 1995
d) El Niño
e) control
f) La Nina
g) El Niño + 2K
h) control + 2K
f) La Nina + 2K
Pressure [hPa]
Longitude
x [10³km]
Relative Humidity [%]

Figure 5.

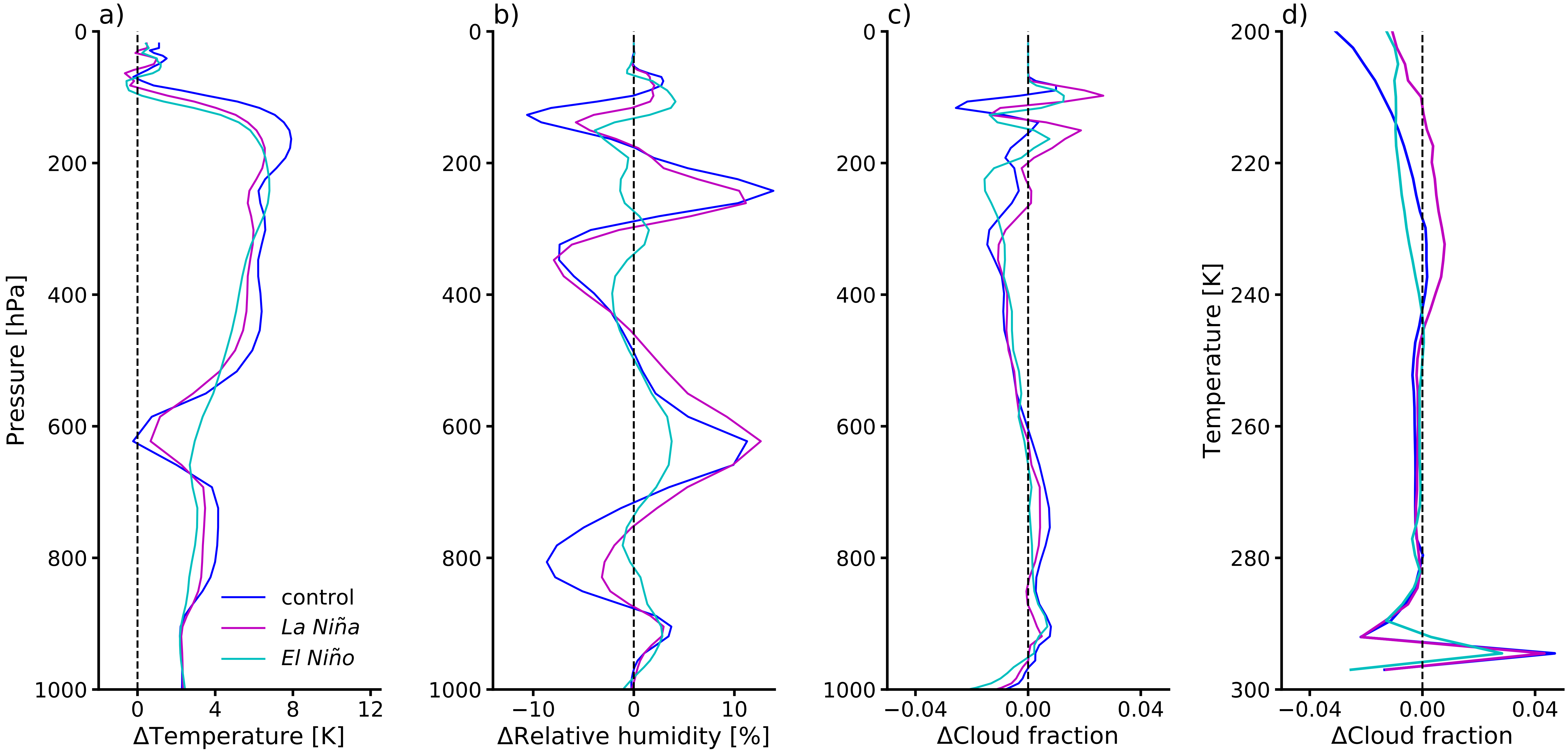

a)
b)
c)
d)
Pressure [hPa]
ΔTemperature [K]
ΔRelative humidity [%]
ΔCloud fraction
ΔCloud fraction
Temperature [K]
control
La Niña
El Niño

Figure 6.

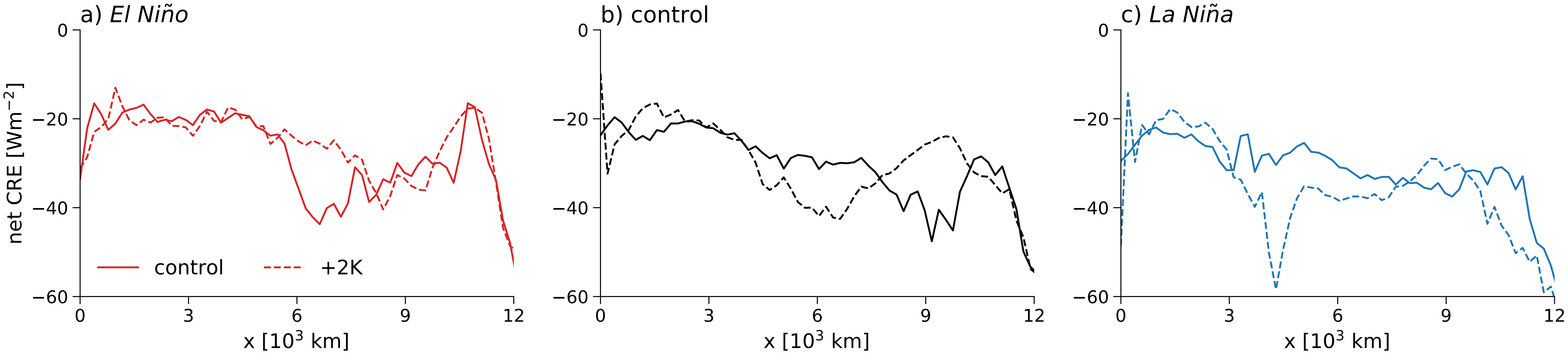
a) El Niño
b) control
c) La Niña
net CRE [Wm^{-2}]
x [10^3 km]
control
+2K
0
−20
−40
−60
0
3
6
9
12

Figure 7.

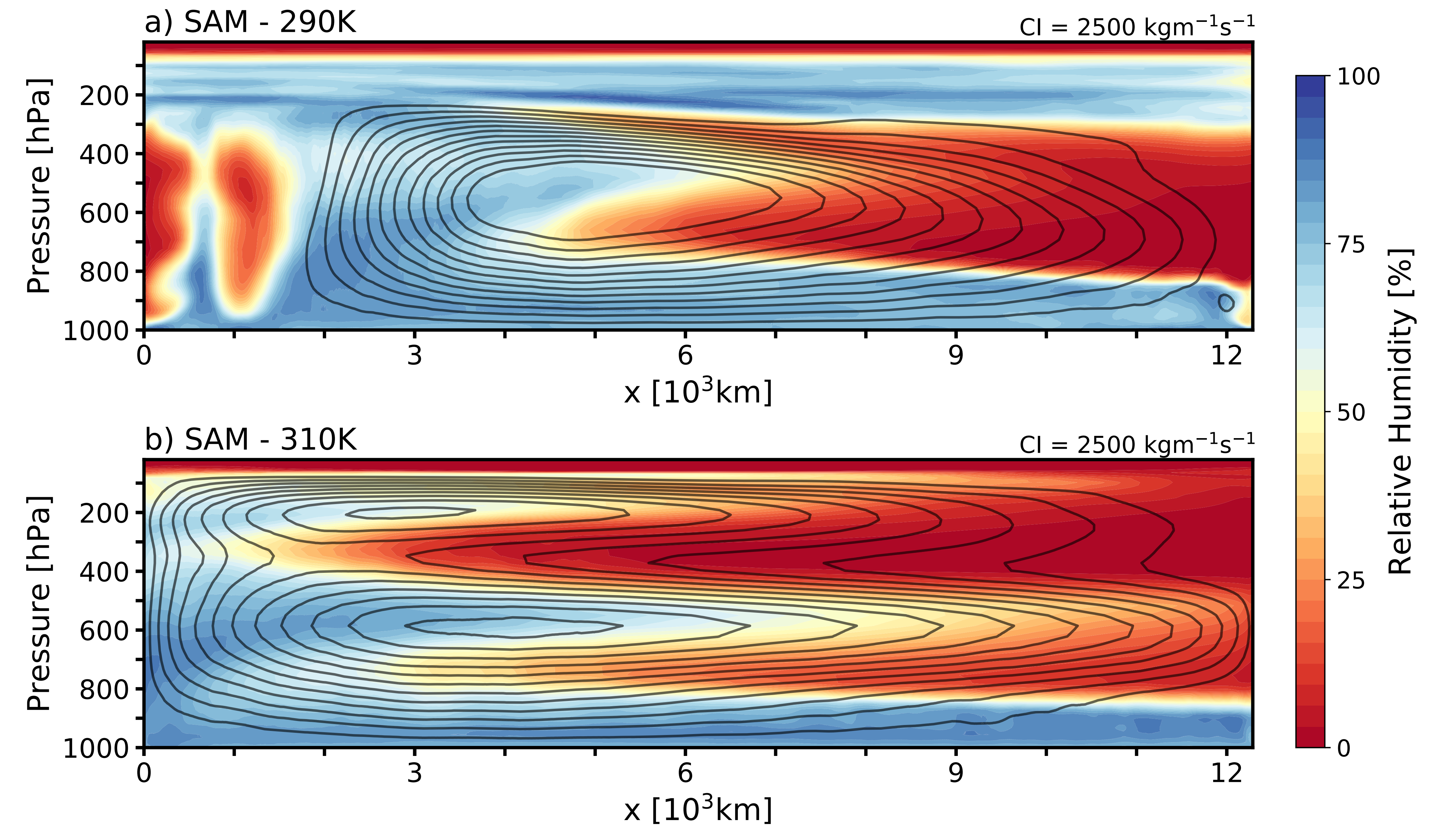

a) SAM - 290K
CI = 2500 kgm^{-1}s^{-1}
Pressure [hPa]
200
400
600
800
1000
0
3
6
9
12
x [10^{3}km]
b) SAM - 310K
CI = 2500 kgm^{-1}s^{-1}
Pressure [hPa]
200
400
600
800
1000
0
3
6
9
12
x [10^{3}km]
Relative Humidity [%]
100
75
50
25
0

Figure 8.

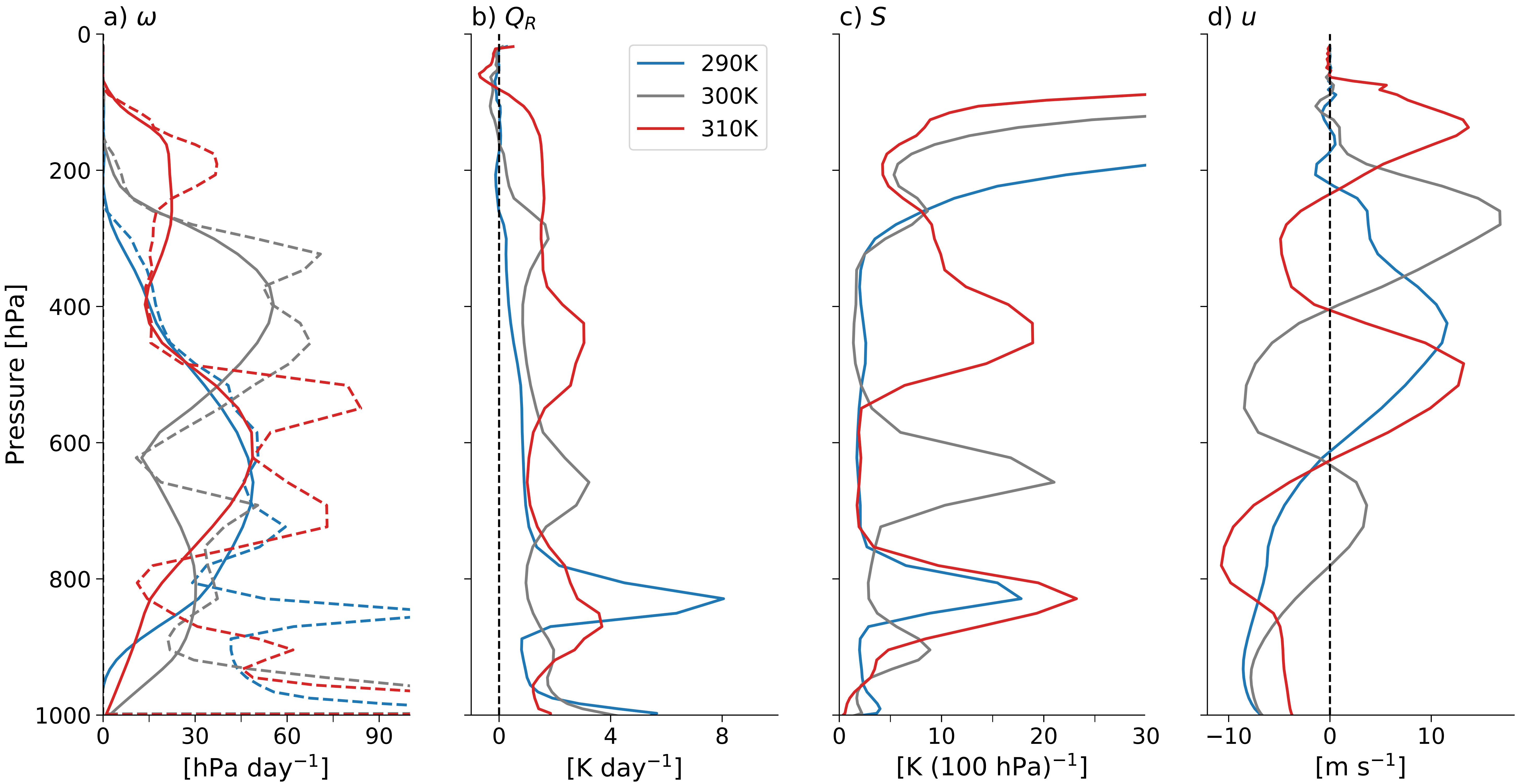
a) ω
b) Q_R
c) S
d) u
Pressure [hPa]
290K
300K
310K
[hPa day^{-1}]
[K day^{-1}]
[K (100 hPa)$^{-1}$]
[m s^{-1}]

Figure 9.

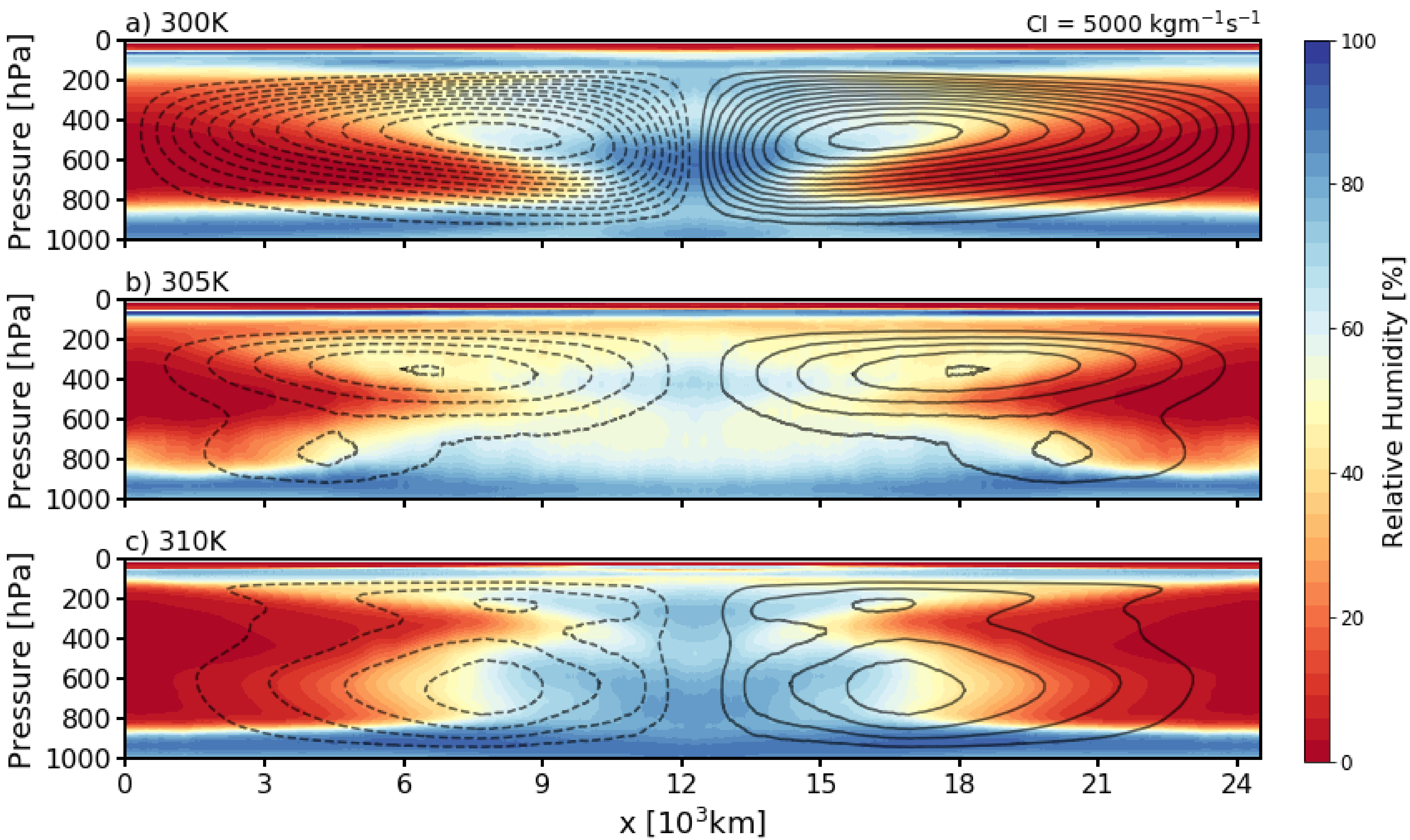

a) 300K
CI = 5000 kgm^{-1}s^{-1}
b) 305K
c) 310K
Pressure [hPa]
0
200
400
600
800
1000
0
3
6
9
12
15
18
21
24
x [10^{3}km]
Relative Humidity [%]
100
80
60
40
20
0

Figure A1.

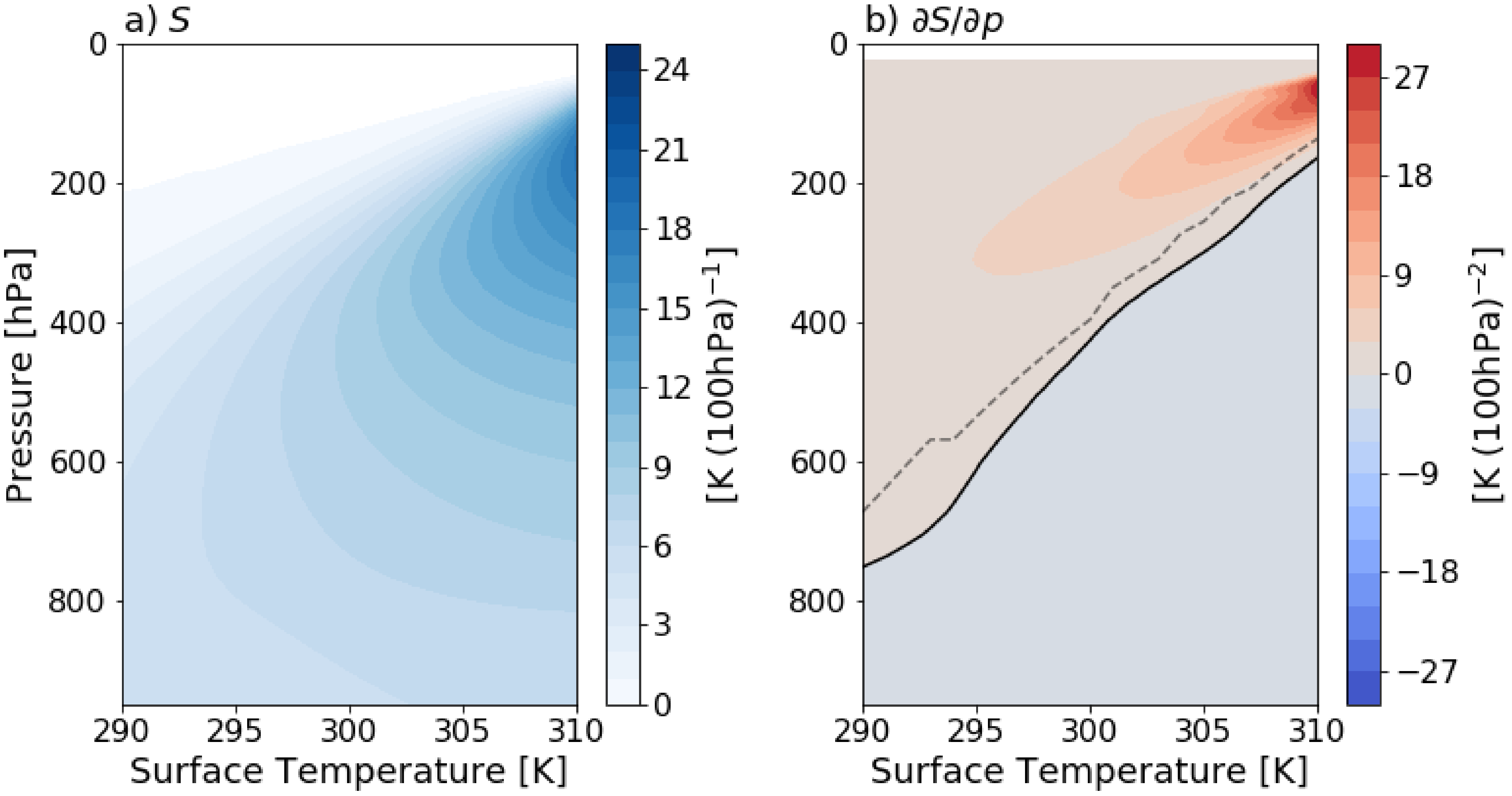
a) S
b) $\partial S/\partial p$
Pressure [hPa]
Surface Temperature [K]
Surface Temperature [K]
[K (100hPa)$^{-1}$]
[K (100hPa)$^{-2}$]
0
200
400
600
800
290
295
300
305
310
0
3
6
9
12
15
18
21
24
27
18
9
0
−9
−18
−27

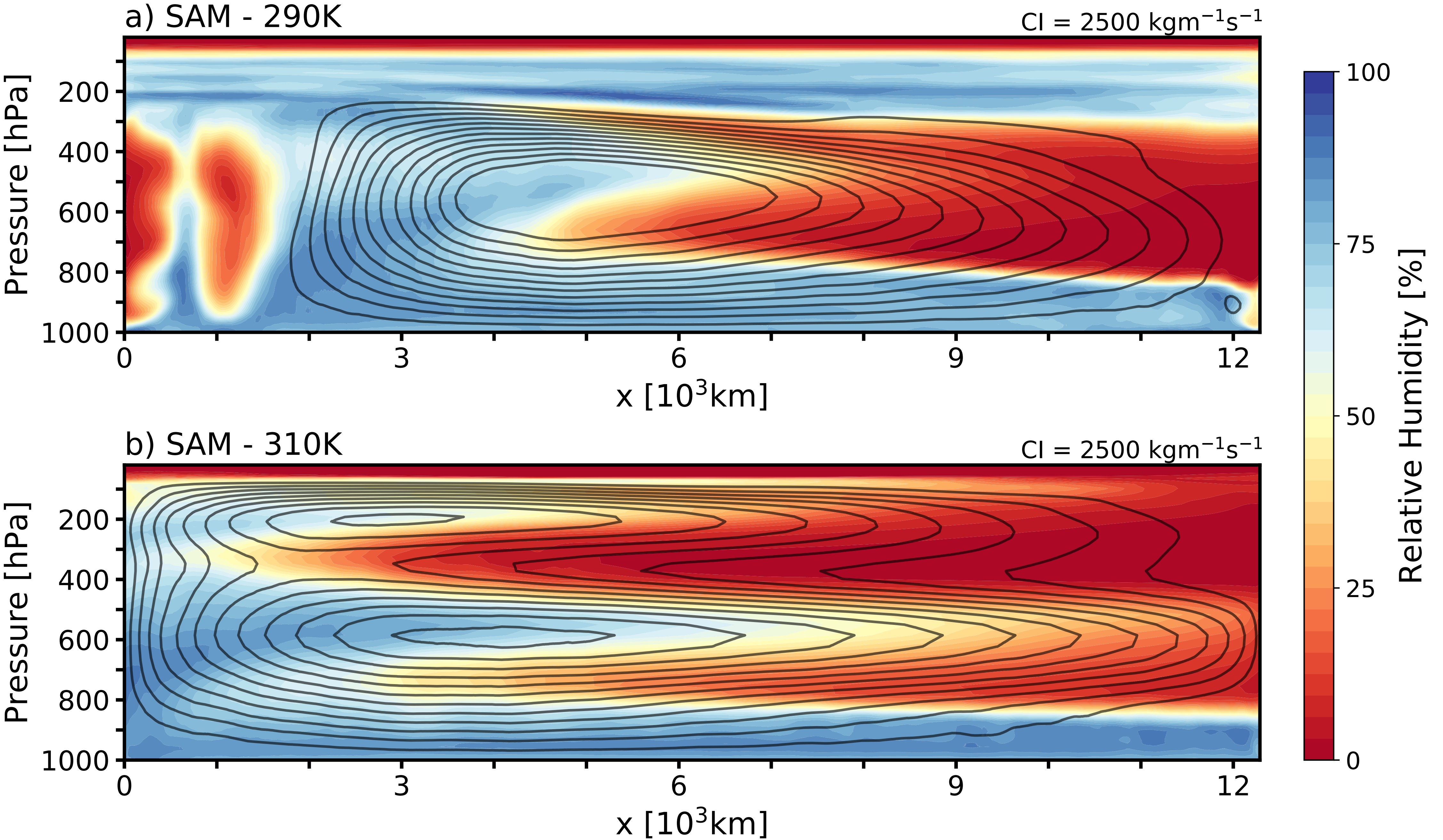

a) SAM - 290K
CI = 2500 kgm⁻¹s⁻¹
Pressure [hPa]
200
400
600
800
1000
0
3
6
9
12
x [10³km]
b) SAM - 310K
CI = 2500 kgm⁻¹s⁻¹
Pressure [hPa]
200
400
600
800
1000
0
3
6
9
12
x [10³km]
Relative Humidity [%]
100
75
50
25
0

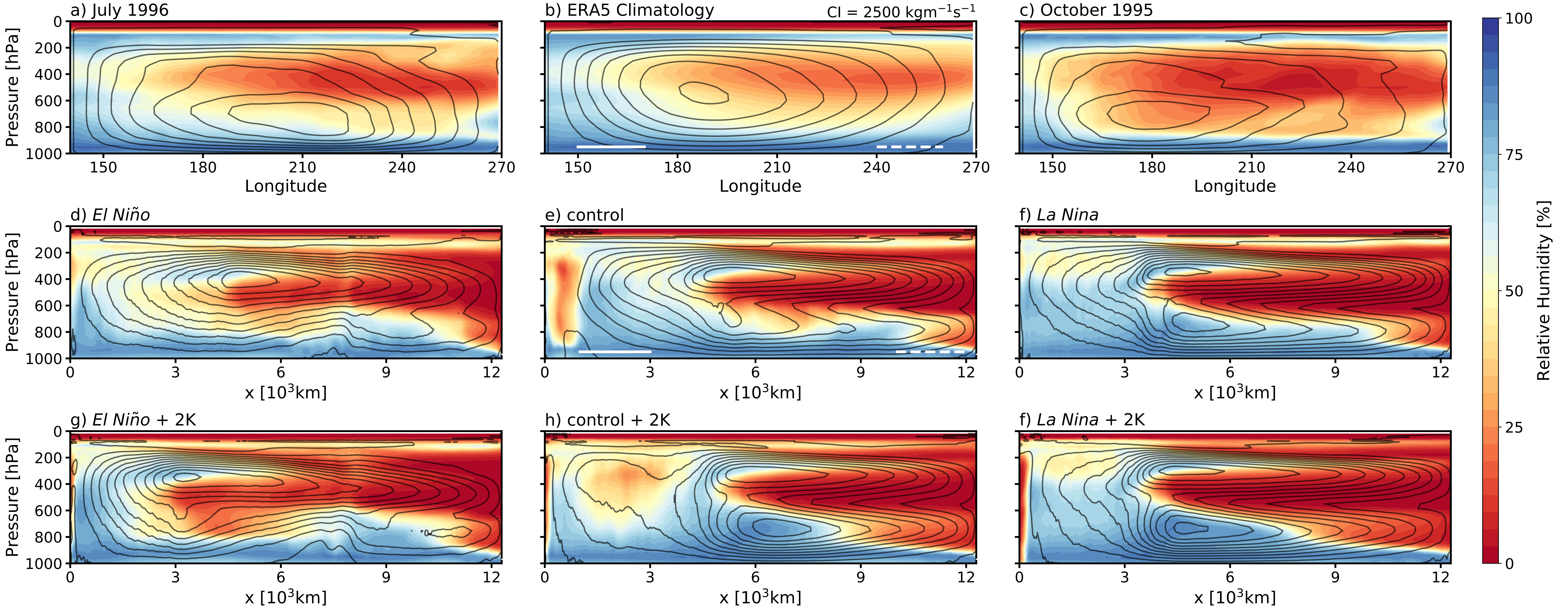

a) July 1996
b) ERA5 Climatology
CI = 2500 kgm⁻¹s⁻¹
c) October 1995
d) El Niño
e) control
f) La Nina
g) El Niño + 2K
h) control + 2K
f) La Nina + 2K
Pressure [hPa]
Longitude
x [10³km]
Relative Humidity [%]